electronics

MDPI

Review

Through-the-Wall Radar Imaging: A Review of Image Reconstruction, Wall Clutter Mitigation, Wall Compensation, and Multipath Processing

Mona Heydari and Reza Khalaj Amineh *

Department of Electrical and Computer Engineering, New York Institute of Technology, New York, NY 10023, USA; mona.heydari@nyit.edu
* Correspondence: rkhalaja@nyit.edu

Abstract

Through-the-wall radar imaging (TWRI) reconstructs objects and structures behind visually opaque barriers using electromagnetic waves. However, image quality is affected by wall reflections, propagation distortion, uncertain wall properties, and multipath interference. This paper reviews TWRI methods with emphasis on image reconstruction, wall-clutter mitigation, wall compensation, and multipath processing. Conventional beamforming, backprojection, diffraction tomography, inverse scattering, holographic imaging, sparse reconstruction, and selected learning-based techniques are examined and compared. The literature indicates that no single reconstruction method provides the best performance under all conditions, as imaging accuracy depends on the acquisition geometry, propagation model, sampling requirements, and target characteristics. Wall-clutter mitigation improves target visibility but does not necessarily correct wall-induced focusing and localization errors. Furthermore, uncertainties in wall thickness and permittivity can introduce coupled propagation errors, while multipath reflections can either generate false targets or provide additional imaging information when properly modeled. The comparison also reveals limitations in existing validation practices, particularly differences in experimental conditions and performance metrics. Promising research directions include joint wall-parameter estimation and image reconstruction, integrated clutter and multipath processing, computationally efficient 3D imaging, and physics-guided reconstruction methods. More realistic experimental validation and consistent evaluation criteria are needed to improve the practical reliability of TWRI systems.

Keywords: through-the-wall radar imaging; image reconstruction; wall clutter mitigation; wall compensation; wall-parameter estimation; autofocusing; multipath processing; inverse scattering; radar image quality

Check for updates

Academic Editor: Massimiliano Pieraccini

Received: 26 October 2026
Revised: 12 November 2026
Accepted: 16 November 2026
Published: 18 November 2026

Copyright: © 2026 by the authors. Licensee MDPI, Basel, Switzerland. This article is an open access article distributed under the terms and conditions of the Creative Commons Attribution (CC BY) license.

1. Introduction

Through-the-wall radar imaging (TWRI) uses electromagnetic (EM) waves to form images of objects and structures located behind visually opaque barriers, such as walls and doors. A radar system transmits signals toward a region of interest and processes the returned fields to estimate the spatial distribution of scattering objects. Unlike methods that only indicate whether a target is present, image reconstruction aims to provide information about target location, shape, and spatial extent. Synthetic aperture beamforming is investigated for through-the-wall imaging by incorporating the effects of wall-induced refraction and changes in propagation speed into the beamformer design [1], while

diffraction-tomographic methods have been developed for three-dimensional (3D) image formation [2]. These capabilities are of interest in search and rescue, security, and the assessment of enclosed or inaccessible environments.

Microwave imaging (MWI) has also been widely investigated for applications such as biomedical imaging, security screening, and non-destructive testing. In particular, recent developments in near-field holographic MWI have demonstrated the possibility of accelerating data acquisition and performing computationally efficient image reconstruction using electronically switched antenna arrays and point-spread functions (PSFs) [3,4]. Although these approaches were developed for general microwave imaging rather than through-the-wall scenarios, they demonstrate advances in acquisition and reconstruction techniques that are relevant to the broader development of radar imaging systems.

Forming a reliable radar image through a wall is more difficult than imaging in free space because the barrier changes both the amplitude and phase of the propagating fields. At the air–wall interfaces, part of the incident field is reflected and part is transmitted. The transmitted field may undergo refraction, attenuation [5], and dispersion, depending on the electrical properties, thickness, and structure of the wall. Internal layers and air gaps can also produce repeated reflections and prolonged returns. If wall propagation effects are ignored or modeled inaccurately, errors in the estimated travel times can reduce the accuracy of coherent image formation [1]. For multilayered walls, a layered-medium Green function can be incorporated into a 3D beamformer to compensate for wall propagation effects [6].

The information available for reconstruction also depends on radar waveform, antenna arrangement, and measurement geometry. Through-wall systems have used pulsed ultrawideband signals, stepped-frequency measurements, and frequency-modulated continuous-wave (FMCW) operation. Spatial data may be acquired by moving an antenna to synthesize an aperture or by using multiple transmitters and receivers. A direct comparison of multiple-input multiple-output (MIMO) and multiple-input single-output (MISO) systems showed that the imaging resolution and acquisition time depend on both the array arrangement and the processing method [7]. Experimental through-wall images have also been obtained using low-cost FMCW radar sensors [8]. Signal bandwidth determines the conventional range resolution, while the antenna aperture size influences cross-range resolution [9]. These factors influence both the quality of reconstructed images and the computational requirements of the imaging process.

Conventional TWRI reconstruction methods include delay-and-sum beamforming and backprojection. They estimate each image pixel by applying the expected propagation delay or phase and combining measurements from different antenna positions. When wall parameters are known, their effects on signal travel times can be incorporated into the beamformer design for coherent through-the-wall image formation. However, coherent summation alone does not remove all sidelobes or artifacts, and imaging errors can occur when the assumed propagation paths are inaccurate. More physics-based approaches formulate image formation as an inverse scattering problem. Under a linearized scattering model, truncated singular-value decomposition has been used to obtain stable reconstructions from through-wall measurements [10]. Three-dimensional diffraction tomography has also been developed by relating measured fields to the spatial-frequency representation of a scene under the Born approximation and applying Fourier-based reconstruction [2]. The accuracy and efficiency of these methods depend on their physical approximations, available measurements, and numerical implementation.

Another direction is sparse and compressive reconstruction, which attempts to reduce the number of measurements required for image formation. The approach is particularly relevant when a scene contains a limited number of significant scattering regions. Compres-

sive sensing has been applied to ultrawideband impulse-radar data to reconstruct point-like and spatially extended targets using fewer samples than conventional full-data imaging [9]. It has also been combined with 3D diffraction tomography to reduce measurement requirements [11]. Because real targets are not always isolated point scatterers, more structured models have been introduced. In particular, a Bayesian compressive-sensing formulation has been used to represent spatial target clusters while accounting for shared support across multipath components [12]. These methods offer a different balance among measurement count, reconstruction assumptions, computational effort, and image quality; the benefits depend on how well the assumed signal structure matches the actual scene.

Strong reflections from the front surface of the wall are another major obstacle to accurate imaging. Wall returns may be much stronger than target returns and can conceal weak targets, especially when they are close to the barrier [13]. Background subtraction can reduce these reflections when measurements of the same scene without the targets are available, but such reference data may be difficult to obtain. Methods that do not require an empty-scene measurement have therefore been investigated. Other methods treat wall returns and target returns as components with different mathematical structure. Low-rank and jointly sparse representations have been used to perform wall-clutter mitigation and polarimetric image formation together [14]. Liu et al. proposed a two-stage robust principal component analysis method combined with backprojection for clutter removal in chaos through-wall imaging radar [15]. The suitability of these approaches depends on whether their assumptions about wall and target responses hold for the measured environment.

Wall-clutter mitigation must be distinguished from wall compensation. The former aims to suppress unwanted wall reflections, whereas the latter aims to correct the propagation model used to focus target returns. For walls with known properties, a layered-medium Green function can be incorporated into 3D beamforming to compensate for wall propagation effects [6]. In practical cases, however, the wall thickness [16], relative permittivity, or internal structure may be unknown. Solimene et al. [17] proposed a two-step approach that first estimates wall thickness and permittivity from radar measurements and then performs 3D imaging using a linear inverse-scattering method. Autofocusing provides another route by adjusting assumed wall parameters according to an image-focus criterion; a recent method investigated how to make this parameter search more efficient [18]. Both approaches seek to reduce defocusing and localization errors, but they differ in the information and optimization procedures they require.

Multipath propagation creates a separate, though related, imaging problem. Signals may return to the radar after reflecting from side walls, floors, ceilings, or other objects, and each indirect path has a different delay. When these paths can be modeled, their returns may provide useful additional information. Wu and co-workers combined a modified Green function with backprojection to associate selected multipath returns with real targets and strengthen reconstructed images [19]. When the indirect paths are instead interpreted as direct target returns, they may create false responses at incorrect locations, commonly called multipath ghosts. A generative adversarial network has been investigated for suppressing such ghosts in radar images, although that study relied on generated training and evaluation data rather than broad validation with measured scenes [20]. Abdalla and co-workers reviewed ghost formation and compared multipath suppression and exploitation methods [21]. Thus, whether multipath should be removed or exploited depends on how accurately the propagation paths can be modeled or identified.

Previous review articles have examined through-the-wall radar imaging from different perspectives. Nkwari et al. provided a general review of radar technologies and through-wall sensing applications [22]. Abdalla and co-workers examined multipath ghosts and their suppression methods [21], while Abdalla reviewed compressive sensing and sparse

image reconstruction [23]. More recent reviews have focused on computationally efficient sparse reconstruction [24] and convolutional neural network (CNN)-based imaging approaches [25]. Although these studies provide valuable discussions of different aspects of TWRI, the present review adopts an imaging-oriented perspective that considers reconstruction algorithms together with the physical and environmental effects influencing reconstructed image quality. In particular, this review compares conventional and advanced reconstruction methods, examines the differences between wall-clutter suppression and propagation compensation, discusses image formation under uncertain wall parameters, and evaluates both multipath mitigation and exploitation. The analysis also considers image resolution, artifacts, localization accuracy, computational requirements, and the strength of experimental validation. Rather than proposing a new reconstruction algorithm, the main contribution is to connect these related technical challenges and provide an evidence-based comparison of the capabilities and limitations of existing TWRI approaches.

2. Review Methodology and Scope

The literature for this review was drawn from an author-assembled collection of approximately 111 publications related to through-the-wall radar sensing and microwave radar imaging. A focused subset was selected for the present review according to its relevance to image formation and to the physical or signal-processing methods that influence reconstructed through-the-wall radar images. The collection includes journal articles, conference papers and related works.

The review focuses on radar image reconstruction of objects and structures behind walls, including both two-dimensional (2D) and 3D imaging. It first considers the effects of wall materials on EM propagation and the acquisition configurations that determine the available imaging data, including synthetic apertures, physical antenna arrays, and different waveform types. The reconstruction methods are classified into conventional beamforming and backprojection, physics-based inversion and tomography, holographic and computational imaging, sparse and compressive reconstruction, and selected learning-based approaches.

3. Fundamentals of Through-the-Wall Radar Imaging

The formation of through-the-wall radar images depends on the measurement geometry and the propagation of EM waves through the intervening wall. The presence of the wall introduces reflection, attenuation, refraction, and additional propagation delays, which can affect the accuracy and quality of reconstructed images. This section presents the basic geometry of TWRI, discusses the effects of wall properties on EM wave propagation and image formation, and introduces the main parameters used to evaluate imaging performance.

3.1. Basic TWRI Geometry

A basic through-the-wall radar imaging arrangement consists of one or more transmitting antennas, receiving antennas, a wall, and an investigation region containing possible targets. The antennas are usually positioned on the accessible side of the wall. A 2D model describes target position by range and cross-range coordinates, whereas 3D imaging also resolves height. The near-field geometry, antenna positions, wall thickness, and target location determine the paths taken by the transmitted and scattered waves [1,26]. Fedeli et al. used a 2D dielectric-slab geometry to formulate the interaction between a wall and hidden dielectric targets, providing an example of how the physical scene is represented in a forward scattering model [27].

For a simple planar-wall model, the propagation of EM waves depends on the antenna positions, wall thickness, and target location. The transmitted waves travel from

the transmitting antenna through the wall toward the target, while the scattered waves return to the receiving antenna. Due to refraction at the air–wall interfaces, the propagation paths may bend, resulting in travel distances and delays that differ from those predicted by a straight free-space path [28]. Zhang considered a 3D multiple-input multiple-output (MIMO) geometry in which transmit–receive pairs illuminate a scene behind single- or multilayered walls [29]. The measurement aperture and positions at which scattered fields are sampled also affect the information available for reconstruction; Maisto et al. showed that nonuniform spatial measurement locations can maintain a PSF close to the continuously sampled reference in their layered-medium model [30].

Figure 1 illustrates the basic geometry of through-the-wall radar imaging and the effects of wall propagation on target localization. As shown in the figure, EM waves travel from the antenna aperture through the wall toward the target, undergoing refraction at the air–wall interfaces. If the imaging algorithm assumes free-space propagation and ignores these effects, the reconstructed target may appear at an incorrect position. Accounting for the wall properties and refracted propagation paths helps reduce this localization error [26]. In practice, antennas may use a physical array, mechanical scanning, or alternative spatial encoding. For example, Li et al. implemented a compact stepped-frequency through-wall radar platform [31], while García-Fernández et al. demonstrated single-channel frequency-diverse computational imaging [32]. Distributed sensors may also view the same hidden target from different locations, providing additional geometry constraints on its position [33]. Regardless of the acquisition approach, coherent image formation requires consistent channel delays and phases, as examined in the multichannel calibration study of Hao et al. [34]. The detailed differences among radar configurations and acquisition schemes are discussed in Section 4.

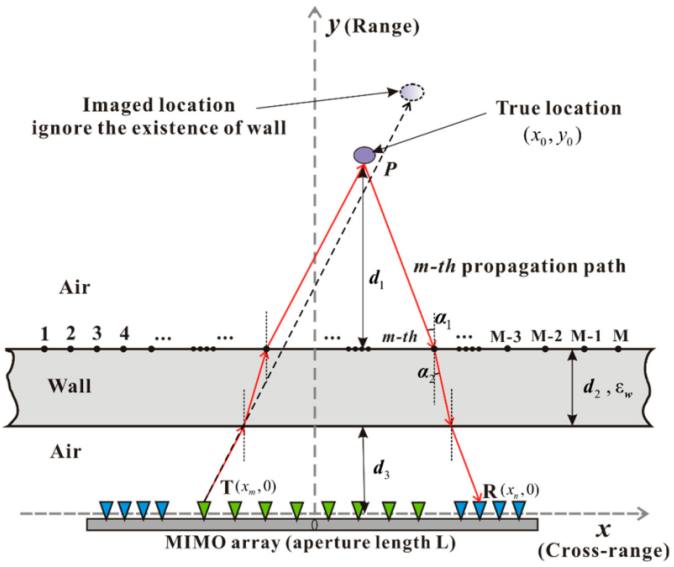


Figure 1. Basic through-the-wall radar geometry showing the antenna aperture, wall, refracted propagation paths, and target-position error when the wall is ignored [26].

3.2. Electromagnetic Wave Propagation Through Walls

When a radar wave reaches a wall, part of the incident field is reflected and part is transmitted into the material. The transmitted field can undergo refraction, phase delay, absorption, and internal reflections before emerging into the room. The relative permittivity ε_r, conductivity σ, thickness d, and internal structure of the wall govern these effects. Measurements and simulations of common materials, including brick and concrete, show that transmission loss varies with wall composition and operating frequency [5]. For a

low-loss, nonmagnetic, approximately homogeneous medium, the phase velocity can be approximated by

$$v_w \simeq \frac{c_0}{\sqrt{\varepsilon_r}}, \quad (1)$$

where c_0 is the free-space speed of light. This expression is a useful first approximation, rather than a complete model for lossy, dispersive, or reinforced walls.

For time-harmonic fields with the $e^{j\omega t}$ convention, the wall's conductive loss may be represented through complex permittivity, $\tilde{\varepsilon} = \varepsilon_0\varepsilon_r - j\sigma/\omega$. The complex propagation constant accounts for both phase advance and amplitude decay. At oblique incidence, Snell's law determines the transmitted direction for an ideal planar interface; the wall-related travel time therefore depends on the incidence angle as well as the material properties. Hu et al. explicitly incorporated refraction and the lower propagation velocity into travel-time calculations for through-wall focusing [26]. Full-wave analysis by Watson et al. investigated multiple-scattering effects using a full-wave-based propagation model that extends beyond the conventional planar layered-wall approximation [35].

Real building walls are not always uniform dielectric slabs. Spatial changes in permittivity and thickness, the presence of reinforcement, and architectural features can introduce additional amplitude and phase variations. Yasmeen and Ram investigated the estimation of electrical characteristics for inhomogeneous walls from scattered fields [36]. Zeng et al. examined wall irregularities such as windows, doors, and pillars when incorporating exterior geometry into wall compensation [37], while Yang et al. studied the recovery of spatially varying wall parameters [38]. In nonuniform-wall simulations and measurements, Zeng et al. investigated multifrequency fusion imaging for nonuniform wall scenarios, addressing the limitations of reconstruction methods that assume uniform wall properties [39]. Heterogeneous walls can also produce wall echoes whose amplitude and phase vary across the aperture or frequency, reducing the validity of simple smooth-wall clutter assumptions [40]. These observations motivate more detailed propagation models but do not imply that every imaging application requires a full-wave solution.

3.3. Effects of the Wall on Image Formation

Radar images are reconstructed by combining the received signals based on a model that describes how EM waves travel between the antennas and the targets. Errors between the assumed focusing delays and the actual propagation delays cause phase misalignment of the target echoes, resulting in image defocusing and potential target localization errors. For a dielectric wall, ignoring the reduced wave speed can shift the apparent target range, while errors in the angle-dependent path can introduce lateral displacement and defocusing [1,26]. Liao et al. combined propagation compensation with coherence-based weighting to address position errors and sidelobe artifacts in 3D MIMO imaging [41]. Li et al. identified medium-path and wavefront-curvature errors as separate contributors to defocusing and position errors in through-wall tomographic Synthetic Aperture Radar (SAR) [42]. These examples show that the observed error depends not only on the wall parameters but also on the imaging geometry and processing assumptions.

Figure 2 compares experimental two-dimensional radar images of two human targets behind a wall, as reported by Hu et al. In Figure 2a, the conventional CC-TDBP algorithm with background subtraction reconstructs both targets, but their estimated positions appear farther from the antenna aperture than their actual positions, indicated by the intersections of the white lines. In Figure 2b, the improved CC-TDBP algorithm accounts for wall-induced propagation effects, bringing the reconstructed target positions closer to their actual locations [26].

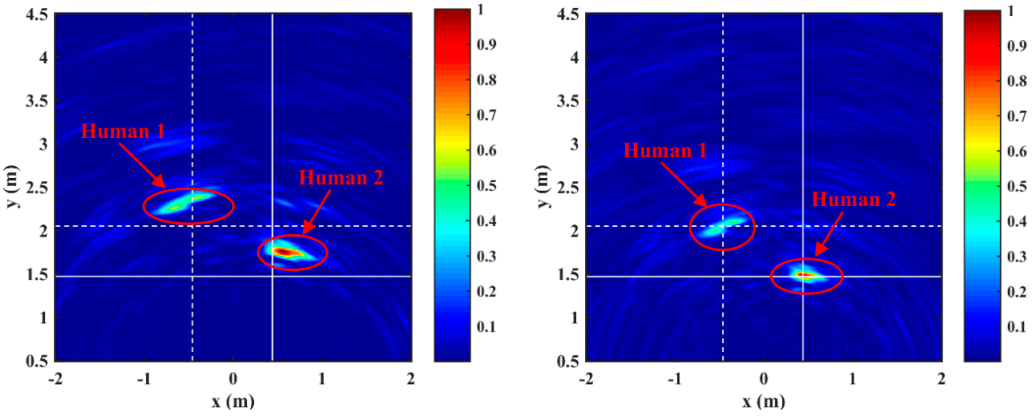


Figure 2. Comparison of experimental two-dimensional through-wall radar images of two human targets: (**a**) conventional CC-TDBP reconstruction with background removal and (**b**) improved CC-TDBP reconstruction accounting for wall propagation effects. Reproduced from Figure 19 of Hu et al. [26].

Another challenge is uncertainty in wall properties. Yao et al. used consistency among distributed radar observations to estimate wall thickness [43]. Strong wall reflections can also obscure weaker target responses. Yang et al. proposed amplitude-coherence-factor weighting to suppress wall clutter in MIMO radar images [44], while Brehier et al. investigated separating wall and target contributions in the presence of heterogeneous noise and outliers [45]. Propagation loss can further reduce the visibility of distant targets, motivating the path-loss compensation approach studied by Mkemwa et al. [46]. Debes et al. also showed that errors in assumed wall parameters can affect the statistical properties of reconstructed radar images used for target detection [47]. These studies demonstrate that a strong image response does not necessarily indicate accurate target localization. Detailed clutter-mitigation, wall-compensation, and autofocusing methods are reviewed in later sections.

3.4. Basic Imaging Performance Concepts

Several quantities are used to describe TWRI image quality, and they assess different aspects of performance. Range resolution indicates how well two scatterers separated in depth can be distinguished. For an ideal monostatic radar in a homogeneous, nondispersive medium, the familiar approximation is $\Delta R \simeq v/(2B)$, where B is the effective bandwidth and v is the wave velocity in that medium. For free space, $v = c_0$; a layered wall–air path generally requires more careful interpretation of this approximation [26,28]. Cross-range resolution refers to the separation of adjacent scatterers perpendicular to the viewing direction and depends strongly on effective aperture, wavelength, target distance, and viewing geometry. Analysis of the sampled PSF by Maisto et al. makes the role of spatial measurement geometry explicit [30]. Dass et al. also investigated 2D and 3D SAR backprojection for detecting objects within and behind walls [48].

The signal-to-noise ratio (SNR) compares a specified target-signal power estimate with the noise power, whereas signal-to-clutter ratio (SCR) compares target energy with unwanted structured returns. Both measures require a clear definition of the evaluation region and whether they are computed before or after image formation. Localization error measures the distance between an estimated target position and its known or independently measured position. Image contrast, PSF width, sidelobe levels, and ghost responses describe complementary aspects of image readability. For example, Xu and Wu evaluated a structure-aware Bayesian reconstruction method in multipath environments, comparing reconstructed

images and normalized mean square error (NMSE) under different measurement sampling rates and noise levels [49].

Table 1 summarizes the main performance concepts introduced here. Comparisons in later sections distinguish physical resolution, apparent sharpness after image processing, target visibility, and geometric accuracy, because improvements in one measure do not automatically establish improvements in the others [30,41,48].

Table 1. Fundamental performance concepts used to evaluate through-the-wall radar images. The definitions are descriptive; numerical comparisons require consistent acquisition conditions and evaluation procedures.

Metric	What It Describes	Important Influences
Range resolution	Minimum practical depth separation of distinguishable responses	Effective bandwidth, propagation speed, dispersion
Cross-range resolution	Minimum practical lateral separation of distinguishable responses	Aperture size, wavelength, target distance, sampling
SNR	Target-signal power relative to noise power	Receiver noise, propagation loss, acquisition conditions
SCR	Target response relative to structured clutter	Wall reflections, room multipath, clutter processing
Localization error	Difference between reconstructed and reference target position	Wall-parameter error, calibration, focusing model
Image contrast	Separation of target brightness from background brightness	Clutter, noise, reconstruction method, display normalization

To relate the imaging performance measures discussed above to different acquisition geometries and reconstruction methods, a common linearized TWRI framework can be considered. A linearized TWRI model can be expressed as

$$\hat{\mathbf{x}} = \mathbf{W}_m \mathbf{A}(\mathcal{G}, \boldsymbol{\theta})\mathbf{x} + \mathbf{W}_m(\mathbf{c} + \mathbf{n}), \tag{2}$$

where $\mathbf{A}$ is the measurement operator determined by the acquisition geometry $\mathcal{G}$ and wall parameters $\boldsymbol{\theta}$, while $\mathbf{W}_m$ represents the linear reconstruction operator associated with method m. The resulting effective imaging operator, $\mathbf{H}_m = \mathbf{W}_m\mathbf{A}$, determines the point-spread response and associated sidelobe artifacts. Consequently, image contrast depends on both the spatial information collected by the radar and the reconstruction method used to process it. For example, wider apertures and additional viewing angles can improve the separation of target responses from background artifacts, while insufficient sampling may introduce ambiguities [7,30]. Conventional beamforming, backprojection, and model-based inversion process these measurements differently, resulting in different sidelobe levels, clutter responses, and reconstructed image contrast. Therefore, improvements in acquisition geometry do not necessarily produce the same contrast improvement across different reconstruction methods.

4. Radar Configurations and Data Acquisition for TWRI

The quality of a through-the-wall radar image depends not only on the reconstruction algorithm but also on which EM field measurements are available. The waveform determines the sampled frequencies and range information, while the transmitting and receiving locations determine the viewing angles and spatial coverage. These choices also affect acquisition time, calibration requirements, and the response to a moving target. For example, Pisa et al. experimentally compared MIMO and multiple-input single-output (MISO) configurations with approximately the same aperture extent, demonstrating differences in

acquisition time and algorithm-dependent cross-range resolution [7]. Therefore, the acquisition configuration must be considered when comparing reconstructed images from different studies.

4.1. Radar Waveforms

Pulsed ultra-wideband (UWB) radar transmits short-duration signals and estimates target range from the measured return delay. A broad effective bandwidth provides the ability to distinguish nearby responses in range, although the useful bandwidth after wall transmission may differ from the transmitted bandwidth. Zhang et al. investigated UWB impulse data for through-wall image reconstruction with reduced measurements [9]. UWB should be understood as a bandwidth designation rather than a separate antenna or array geometry: wideband information may also be collected with a frequency-stepped or chirped waveform [26]. Wall-induced attenuation can affect range and cross-range resolution differently. Range resolution depends mainly on the effective signal bandwidth, so the loss of usable frequency components may reduce range resolution. In contrast, cross-range resolution depends primarily on the effective antenna aperture, wavelength, and viewing geometry [50]. Therefore, a reduction in usable bandwidth does not directly affect cross-range resolution in the same way. However, if higher frequencies experience greater attenuation, the effective operating wavelength may increase, which can reduce cross-range resolution. Wall refraction and propagation distortion may also affect cross-range focusing [1,5].

Stepped-frequency continuous-wave (SFCW) radar sequentially measures the complex response at discrete frequencies, often using a vector network analyzer or a coherent frequency synthesizer. When these frequencies are uniformly spaced, a range profile can be obtained by an inverse Fourier transform after suitable calibration and windowing. Narayanan et al. investigated MIMO radar imaging of single and multiple targets through different wall configurations [51]. Hu et al. combined SFCW operation with a sparse UWB MIMO array and obtained measured 2D images of stationary targets through brick and concrete walls [26]. More recently, Li et al. developed a compact dual-channel software-defined-radio SFCW system and addressed phase incoherence between channels [31].

Frequency-modulated continuous-wave (FMCW) radar uses a continuous frequency sweep. Mixing the transmitted and delayed received signals produces a beat signal whose frequency contains range information, subject to the waveform and receiver model. An S-band FMCW prototype with one transmitter and two receivers was experimentally evaluated for through-wall range–angle–Doppler estimation [52]. Maaref and Millot implemented a wideband FMCW array-based system for imaging and localizing people behind a wall [50]. Paun demonstrated synthetic-aperture imaging with a low-cost K-band FMCW module and reported a through-wall experiment with a metal object behind a thin wooden-fiberboard barrier [8]. This result supports the feasibility of low-cost equipment in the tested configuration, but should not be generalized to thick or highly conductive walls.

The waveform categories in Figure 3 represents different methods of transmitting and measuring radar signals.A short impulse occupies a broad spectrum in a single emission, SFCW samples this spectrum at discrete frequency steps, and FMCW measures a swept-frequency response. For N_f uniformly spaced frequency samples separated by Δf, the frequency span is $B = (N_f - 1)\Delta f$. The corresponding delay ambiguity period is $1/\Delta f$, which gives an unambiguous range interval of $R_{\text{amb}} = c_0/(2\Delta f)$ for an ideal monostatic radar in free space. These relations provide first-order acquisition guidelines; window functions, antenna responses, missing frequency samples, wall dispersion, and phase calibration can affect the measured range response [26,31]. Table 2 summarizes the principal trade-offs.

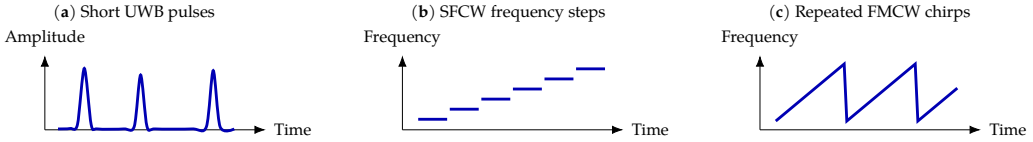


Figure 3. Conceptual comparison of common radar waveforms: (**a**) pulsed ultra-wideband (UWB) radar, showing short-duration pulses in the time domain; (**b**) stepped-frequency continuous-wave (SFCW) radar, showing discrete frequency steps; and (**c**) frequency-modulated continuous-wave (FMCW) radar, showing repeated frequency sweeps. The diagrams illustrate the waveform principles and are not drawn to scale.

Table 2. Comparison of waveform options used in through-the-wall radar measurements. The limitations depend on the implementation and should not be interpreted as universal performance rankings.

Waveform	Acquisition Principle and Useful Features	Main Requirements and Limitations
Pulsed UWB	Short-duration pulses; wide effective bandwidth; time-domain delay information [9]	Requires suitable fast-time acquisition; sensitive to pulse distortion and wall propagation effects.
SFCW	Coherent complex measurements at discrete frequencies; adjustable frequency coverage [26]	Sweep duration and phase coherence must be considered; channel phase errors may require compensation [31].
FMCW	Continuous frequency sweeps with beat-frequency processing; compact radar hardware is available [8,52]	Requires suitable sweep calibration and phase stability for coherent aperture-based imaging.

4.2. Transmitter–Receiver Configurations

Radar measurements are also classified by the placement of the transmitter (Tx) and receiver (Rx). In monostatic acquisition, transmission and reception are colocated, or approximated as colocated, and the two-way target path can often be described by one antenna position. In bistatic acquisition, Tx and Rx occupy different positions, while multistatic acquisition combines several separated transmit–receive paths. The latter provides additional viewing diversity, but each path can interact with the wall differently. A bistatic passive-SAR configuration using external signals was analyzed for single- and multilayer walls by Abedi and Zakeri [53]. Watson et al. developed a multistatic through-wall SAR image formulation that accounts for full-wave transmission and multiple-scattering effects associated with the wall [35].

A single-input single-output (SISO) radar obtains one Tx–Rx channel at a time. Single-input multiple-output (SIMO), MISO, and MIMO designs use several receiving elements, transmitting elements, or both. For N_t transmitters and N_r receivers, a fully measured MIMO acquisition can provide up to N_tN_r distinguishable transmitter–receiver channels; this is a count of channels, not necessarily a count of independent image-resolution cells. Boudamouz et al. reported numerical and measured MIMO beamforming results through a cinder-block wall [54]. Narayanan et al. examined virtual arrays and reconstructed single- and multiple-target scenes using measured data [51]. Lu et al. studied how a split-transmit arrangement can realize a desired virtual aperture with reduced physical aperture length, assessing the effect using the PSF and through-wall measurements [55].

A greater nominal number of virtual channels does not automatically imply better imaging. Array redundancy, missing spatial frequencies, element pattern, mutual coupling, wall-dependent phase, and the image-formation algorithm also matter. Pisa et al. compared 16 equivalent MIMO channels with a 10-antenna MISO arrangement, finding that the latter acquired data in roughly half the time in their experimental setup while providing lower cross-range resolution under their Fourier-transform reconstruction [7]. For coherent MIMO imaging, systematic interchannel delay and phase differences must be calibrated; Hao et al.

specifically addressed this requirement in a through-wall multichannel system [34]. This trade-off motivates selecting the array according to the desired field of view, target motion, and available acquisition time rather than transmitter and receiver counts alone.

4.3. Aperture and Scanning Geometries

Synthetic aperture radar (SAR) measures the target response at multiple antenna locations and combines them to create an effective larger aperture. A single antenna or a small number of antennas can be translated along a line or across a plane, which reduces the number of simultaneous RF channels but requires accurate knowledge of measurement positions and phase. In earlier through-wall SAR work, wall-aware beamforming was demonstrated using a synthetic aperture [1]. Corbett et al. also showed, using simulations and measurements, that target vibration can introduce additional paired-echo artifacts in through-wall SAR imagery [56]. Paun's FMCW experiment illustrates that such scanning can be implemented with a low-cost radar front end, provided the moving measurement geometry is controlled [8].

Physical arrays obtain data with multiple antenna elements without requiring the entire aperture to move during each image frame. Their principal trade-off is the additional RF hardware, switches, interconnections, or multiplexing required. Hu et al. demonstrated a sparse linear MIMO array that acquired 64 virtual channel measurements from 16 physical antenna elements [26]. A switched 2D MIMO array for imaging a human body in different postures was analyzed by Liu et al. [57]. Ranjbaran and Mohanna constructed a 19-element hexagonally arranged array for 3D through-wall microwave imaging of conductive objects [58]. These examples show that array geometry is selected jointly with the required image dimensions and propagation model, not simply by maximizing the antenna count.

Figure 4 illustrates two common acquisition geometries used in TWRI. In Figure 4a, the radar collects measurements sequentially at different antenna positions to synthesize an aperture. In Figure 4b, multiple transmitting and receiving antennas provide different measurement channels without mechanically scanning the complete aperture. The choice between these configurations affects acquisition time, hardware requirements, and spatial sampling [1,7,26].

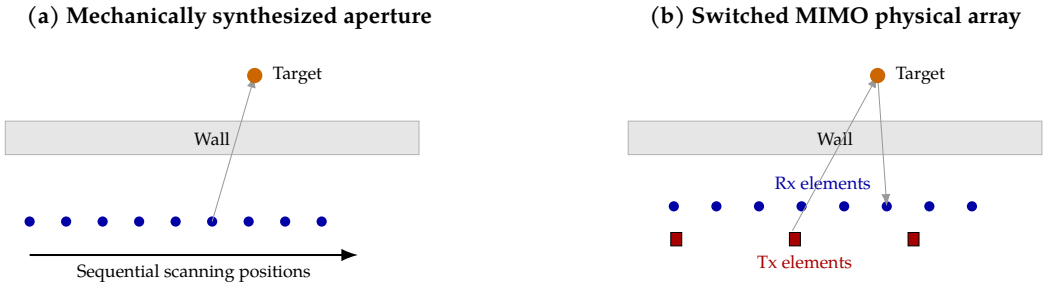


Figure 4. Conceptual comparison of antenna aperture configurations for through-the-wall radar imaging: (**a**) a mechanically synthesized aperture formed by sequential measurements at different antenna positions and (**b**) a physical MIMO array using multiple transmitting and receiving elements. The diagrams illustrate the acquisition geometries and are not drawn to scale.

A linear aperture primarily samples one cross-range direction and is commonly used to form a range–cross-range image. A planar aperture adds measurements in a second transverse direction to support 3D reconstruction, while other geometries may be chosen to suit a particular region of interest. Zhang described 3D through-wall imaging using a MIMO radar [29]. Pan et al. implemented a sparse, 2D UWB MIMO array and reported 3D through-wall imaging of stationary and moving targets, using a reference channel to help address motion effects [59]. A later study by Pan et al. examined motion compensation for

time-division-multiplexed sparse MIMO acquisition [60]. Accordingly, a physical planar aperture may shorten acquisition compared with a complete mechanical scan, but sequential channel switching can still introduce motion-related phase inconsistencies.

Geometry may also be diversified through multiple viewing locations instead of enlarging one aperture. Ahmad and Amin investigated fusion of synthetic-aperture views obtained from different locations around an urban structure [61]. Jia et al. used multiple channels and viewing directions for building-layout imaging [62], and subsequently proposed two single-side spotlight locations for observing complementary building corners and stationary targets [63]. The corresponding images must be registered and combined appropriately; multiview image-fusion strategies were evaluated using measured data by Seng et al. [64] and later examined for weak-target preservation by Chen and Chen [65].

When radar images are obtained from different spotlight locations, accurate spatial registration is required before image fusion. The images can be aligned using known radar positions and a common scene-coordinate system, as illustrated by the two-location imaging approach of Jia et al. [63]. When common targets or building features are visible, registration accuracy can be evaluated using the root mean square error (RMSE) of corresponding target or landmark positions. For overlapping image regions, normalized cross-correlation or mutual information can also be used to assess image alignment. However, these similarity measures may become unreliable when the spotlight views contain different scattering features or have little spatial overlap. Therefore, registration accuracy should be evaluated separately from the improvements in image contrast and target visibility obtained after fusion [64,65].

These studies illustrate the potential of multiview acquisition and image fusion to combine complementary observations of the same scene, although successful reconstruction depends on accurate image registration and the selected fusion method.

4.4. Near-Field and Far-Field Configurations

In many portable through-wall experiments, the antenna–wall separation and target distance are not large compared with the aperture dimensions. Consequently, a point in the scene can have noticeably different path lengths to different antennas. Near-field image formation must then account for wavefront curvature and, where appropriate, the different transmit and receive paths through the wall. In contrast, far-field approximations describe the spatial dependence of propagation more simply, but may introduce focusing errors when applied outside their valid geometry. Boudamouz et al. explicitly considered near-field propagation in a through-wall MIMO beamforming study [54]. Jin and Yarovoy used an array-based wall-aware formulation for locating targets with measured data, illustrating the need to account for wall geometry together with the acquisition geometry [66].

The Fraunhofer distance $R_F \approx 2D^2/\lambda$, with aperture extent D and free-space wavelength λ, is a useful free-space guide for a simple aperture but is not a complete through-wall focusing criterion. A layered wall introduces transmission and refraction effects, and a wideband system operates at many wavelengths. For this reason, wideband PSFs are often more informative than a single far-field beamwidth when assessing through-wall array performance. Lu et al. examined the near-field PSFs of a virtual aperture [55]. Maisto et al. optimized nonuniform measurement locations for a layered-medium through-wall configuration so that the sampled PSF approximated that of a continuous aperture, under their stated linearized model [30]. Near-field holographic imaging provides another approach to TWRI reconstruction. Heydari and Amineh investigated a wideband near-field holographic method that uses wall-dependent PSFs to reconstruct objects behind dielectric barriers. Their study also addressed uncertainty in wall thickness by comparing reconstructions from different frequency subsets using the structural similarity (SSIM) metric. Numerical

simulations and experimental measurements through wooden walls demonstrated the proposed approach for reconstructing objects under wall-thickness uncertainty [16]. These analyses support evaluating both sampling density and acquisition geometry against the intended scene depth.

Near-field requirements also affect more recent computational imaging configurations. García-Fernández et al. investigated a single-channel frequency-diverse system that obtains spatial information through frequency-dependent illumination rather than a conventional densely sampled antenna array [32]. Although it reduces the number of conventional receiver channels, its spatial encoding still requires an appropriate forward model and calibration.

4.5. Acquisition Requirements and Practical Trade-Offs

The first acquisition requirement is a frequency range that balances useful range resolution with propagation loss through the barrier. As reviewed in Section 3, the ideal homogeneous-medium approximation $\Delta R \simeq v/(2B)$ describes bandwidth-controlled range separation but does not by itself predict resolution after passage through a dispersive wall. Waveform measurements should therefore report the transmitted and effective usable bandwidth, the center frequency, and the wall material and thickness. For example, Paun demonstrated through-wall synthetic-aperture imaging using a low-cost K-band FMCW radar and a 3-cm-thick medium-density fiberboard wall [8]. In contrast, Heydari and Amineh investigated wideband near-field holographic imaging through wooden walls using a PSF-based reconstruction approach that also addressed uncertainty in wall thickness [16]. These studies demonstrate different acquisition and reconstruction conditions.

Second, spatial sampling should be considered together with the effective aperture. Sparse arrays can reduce the number of physical channels but can generate grating lobes and strong sidelobes if the sampled spatial frequencies are insufficient. Liu et al. examined sign-coherence-based grating-lobe suppression for a sparse MIMO through-wall array [67]. Muqaibel et al. investigated Pythagorean subapertures for improving the separation of genuine target responses from aspect-dependent multipath ghosts, based on synthetic and electromagnetic-simulation data [68]. In a different direction, Maisto et al. showed that a nonuniform measurement arrangement can reproduce the reference PSF with fewer samples for the particular layered-medium forward model they analyzed [30]. These results should not be combined into one numerical ranking because they use different scene models and evaluation procedures.

Third, practical acquisition requires stable channel phase, accurate scan positions, time synchronization, and suitable treatment of wall and system responses. The phase-compensation study of Li et al. [31] and multichannel calibration study of Hao et al. [34] illustrate this need for stepped-frequency and switched-MIMO systems, respectively. Full-polarimetric measurements provide another acquisition dimension; Zhang et al. collected multiple polarization channels and incorporated a layered-medium response into image formation [69]. The benefit of additional polarization data depends on the targets and on the calibration required across polarization channels.

Table 3 compares selected experimental and numerical studies with different acquisition choices. The entries intentionally identify the validation context; a result obtained with simulated point targets cannot establish the performance of a hardware system in a realistic building. Likewise, reporting a fast scan does not by itself establish real-time imaging unless the acquisition, transfer, calibration, and reconstruction times are all considered.

Table 3. Representative through-wall acquisition studies and the limits of their comparisons. The table focuses on acquisition and validation, not a ranking of reconstruction algorithms.

Study	Acquisition Configuration	Evidence and Comparison Limitation
Heydari et al. [16]	Wideband near-field holographic imaging with wall-dependent PSFs	Numerical and experimental evaluation through wooden walls; wall-thickness uncertainty considered
Hu et al. [26]	SFCW, sparse linear UWB MIMO array	Experimental 2D imaging through brick and concrete; specific array and focusing method
Pisa et al. [7]	Compared MISO and MIMO arrangements	Experimental acquisition-time and resolution comparison under matched study conditions
Li et al. [31]	Dual-channel SDR SFCW radar	Hardware demonstration and phase-coherence treatment; not a broad comparison of imaging arrays
Paun [8]	Low-cost FMCW with synthetic scanning	Experimental imaging behind thin fiberboard; not evidence for thick-wall penetration
Pan et al. [59]	Switched planar UWB MIMO and reference channel	Experimental 3D scenes including target motion; dependent on compensation model
Ranjbaran and Mohanna [58]	Switched hexagonal antenna array	Experimental 3D imaging of conductive objects behind dielectric layers
Maisto et al. [30]	Optimized nonuniform spatial sampling	Layered-medium numerical PSF study; not a direct hardware validation
Jia et al. [63]	MIMO radar at two spotlight locations	Numerical building-corner and target imaging; not a full-scale experimental comparison

It is important to distinguish hardware and data acquisition limitations from reconstruction algorithm limitations. Hardware and acquisition factors, including bandwidth, antenna aperture, spatial sampling, channel calibration, and measurement noise, determine the amount and quality of information available for image reconstruction [7,26,30]. For example, limited bandwidth affects range resolution, while a restricted aperture reduces the available spatial information. These limitations cannot always be overcome by improving the reconstruction algorithm alone. In contrast, reconstruction algorithms introduce additional limitations through their physical assumptions, mathematical models, and computational requirements.

In addition to conventional radar systems, wireless communication signals have been investigated for through-wall imaging. Depatla et al. [70] used Wi-Fi power measurements and a Rytov-based propagation model to reconstruct hidden structures. Karanam and Mostofi [71] extended wireless imaging to 3D using measurements collected by unmanned aerial vehicles. Guo et al. [72] investigated radio tomographic imaging using received signal strength and regularization to reconstruct building layouts. Similarly, Zhang et al. [73] developed an iterative reconstruction method using commercial Wi-Fi signals. More recently, channel state information (CSI) has been investigated for image reconstruction. Strohmayer et al. [74] used Wi-Fi CSI and a learning-based method to generate images in through-wall scenarios. Bazzi et al. [75] proposed 3D environmental imaging using CSI-derived multipath information and ray tracing. Li et al. [76] further investigated 3D reconstruction using sparse multi-view CSI and a neural scattering-field model. Although the latter ISAC methods have not been established as conventional through-wall radar imaging techniques, they demonstrate the potential of wireless communication measurements for spatial reconstruction. Their application to complex through-wall environments requires further investigation.

In summary, waveform type, channel geometry, aperture sampling, and calibration jointly influence the information available for TWRI reconstruction. Comparisons between reconstruction methods should therefore account for differences in acquisition conditions

and experimental validation rather than attributing all differences in image quality to the reconstruction algorithms alone. The next section reviews the main image reconstruction methods used to process these measurements.

5. Image Reconstruction Methods

Image reconstruction converts radar measurements into a spatial representation of the scene behind a wall. The measured echoes contain information about the locations and scattering properties of hidden objects, but they are also affected by the antenna arrangement, signal bandwidth, and propagation through the barrier. Different algorithms use this information in different ways. Conventional methods focus the measured fields by compensating for the expected travel time, whereas model-based methods relate the data to a scattering distribution through a forward operator. Sparse methods add prior assumptions about how the targets occupy the image domain. These approaches are closely related, but they differ in their physical assumptions, computational requirements, and interpretation of the final image [1,9,10].

In this section, the emphasis is on how an image is formed from available measurements. Wall-clutter removal, estimation of unknown wall parameters, and multipath suppression are discussed in Sections 6–8. When comparing reconstruction methods, it is important to distinguish visual image sharpness, spatial resolution, and target localization accuracy. These measures describe different aspects of reconstruction performance, and improvement in one does not necessarily indicate improvement in the others [30,49].

5.1. Delay-and-Sum and Conventional Beamforming

Delay-and-sum (DAS) beamforming is one of the most direct approaches to TWRI. For each candidate image position, the algorithm predicts the propagation time from the transmitting antenna to that position and from the position to the receiving antenna. The received signals are shifted by the corresponding delays and then added coherently. A target located near the assumed position tends to contribute consistently across the aperture, whereas echoes originating elsewhere combine less coherently. Ahmad et al. developed a synthetic-aperture beamformer that explicitly incorporated refraction and the reduced propagation speed inside a dielectric wall [1]. Three-dimensional wideband beamforming subsequently extended wall-aware focusing to a volumetric investigation region [28]. A further MIMO formulation supported volumetric imaging from multiple transmitter–receiver pairs [29].

For time-domain data, a representative delay-and-sum image can be expressed as [1,26]

$$I_{\mathrm{DAS}}(\mathbf{r}) = \left| \sum_{m=1}^{M} w_m(\mathbf{r})\, s_m(\tau_m(\mathbf{r};\boldsymbol{\theta}_w)) \right|, \tag{3}$$

where $\mathbf{r}$ is a trial target location, M is the total number of measurement channels, $s_m(t)$ is the calibrated return for channel m, $w_m(\mathbf{r})$ is a weighting function, and $\tau_m(\mathbf{r};\boldsymbol{\theta}_w)$ is the predicted two-way propagation delay calculated using the assumed wall parameters $\boldsymbol{\theta}_w$. Equation (3) represents a general DAS focusing formulation rather than the exact implementation of a particular study.

DAS is attractive because it is physically intuitive and does not require solving a large inverse problem. It also allows changes in measurement geometry to be represented directly through the travel-time model. Boudamouz et al. investigated MIMO beamforming in a through-wall geometry, including numerical and experimental aspects of the imaging response [54]. Zhang et al. incorporated polarization channels into the beamforming formulation, showing that the reconstruction operator can be extended beyond a single scalar measurement component [69]. Nevertheless, conventional DAS may produce broad

target responses and sidelobes when the aperture is limited or sparsely sampled. Alternative reconstruction and weighting techniques have been investigated to improve image formation. Cicchetti et al. compared conventional DAS with Fourier-transform, MUSIC, and hybrid reconstruction methods [77]. Guo et al. investigated adaptive beamforming based on physical subspace partitioning [78], while Yang et al. proposed imaginary sign coherence-factor weighting to suppress grating lobes and sidelobes in through-wall radar images [79].

5.2. Back-Projection Methods

Back-projection (BP) reconstructs radar images by mapping received signals to candidate target positions according to their expected propagation delays and coherently combining contributions from different measurement channels. In its time-domain form, BP is closely related to DAS beamforming. It can accommodate different antenna geometries and wall-dependent propagation paths, although direct reconstruction becomes computationally expensive for large 3D scenes [1,48]. Dehmollaian and Sarabandi investigated refocusing SAR images affected by wall-induced propagation distortions [80].

Hu et al. developed a cross-correlation-based time-domain BP (CC-TDBP) algorithm incorporating wall propagation effects and demonstrated 2D imaging of stationary human targets behind brick and concrete walls [26]. Dass et al. investigated 2D and 3D SAR backprojection for objects within and behind walls [48]. Paun demonstrated low-cost FMCW-based SAR imaging of metallic targets behind a 3-cm medium-density fiberboard wall [8]. Figure 5 illustrates an experimental reconstruction from this study.

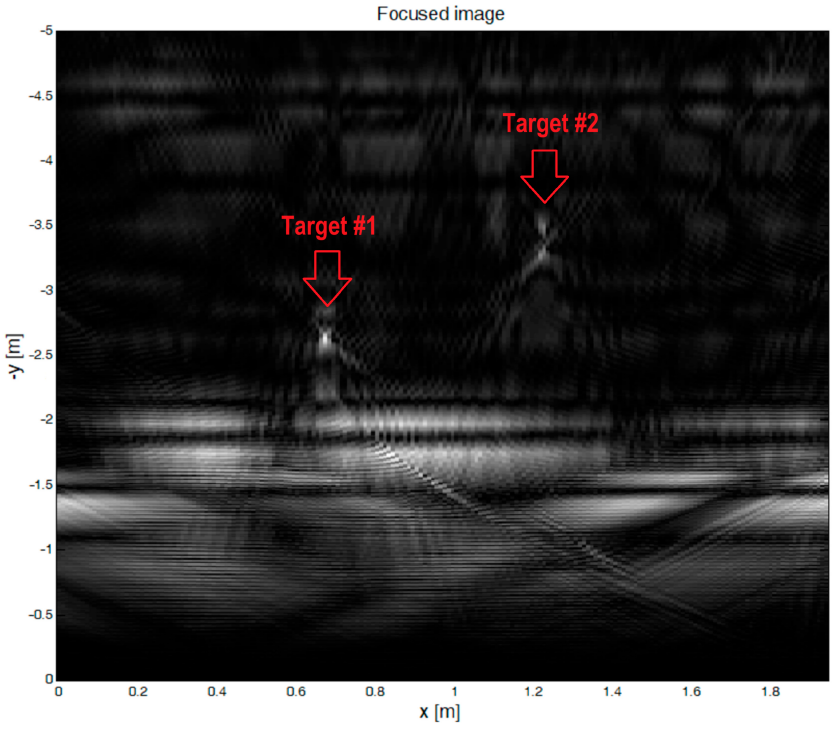


Figure 5. Experimentally focused through-wall SAR image obtained with a low-cost FMCW system. Reproduced from original Figure 14 of Paun [8], Remote Sensing (2024), under the Creative Commons Attribution 4.0 license (CC BY 4.0). The original experiment used metal targets behind a 3 cm MDF wall.

The computational cost of BP depends on the image-grid size, number of measurement channels, and signal samples. Although BP is flexible, its accuracy depends on the propagation model, while its computational requirements increase for larger imaging volumes. Wall-parameter uncertainty and its compensation are discussed in Section 7.

For practical comparison, the BP runtime depends on the number of image pixels, channels, and frequency or time samples, as well as on interpolation and acceleration strategies. Paun's experiment demonstrates that relatively inexpensive hardware can support SAR focusing for a particular thin-wall configuration; it should not be taken as evidence that the same radar frequency penetrates thick or highly lossy walls [8]. A detailed treatment of correcting the travel-time model when the wall properties are uncertain is deferred to Section 7.

5.3. Frequency-Domain and Migration Methods

Frequency-domain reconstruction uses complex radar measurements collected at different frequencies and antenna positions. When the acquisition geometry supports a suitable spectral representation, Fourier transforms can reduce the computational requirements of image formation. Migration methods map measured spatial-frequency components to the wavenumber domain of the reconstructed scene. However, the reconstruction operator must account for wall propagation effects, since free-space approximations may introduce focusing and localization errors [6,77]. Cicchetti et al. compared DAS, Fourier-transform (FT), MUSIC, and hybrid reconstruction methods using simulated and measured data. Their FT-MUSIC approach reduced execution time compared with DAS-MUSIC under the investigated conditions [77]. Testa et al. later investigated computationally efficient implementations using Fourier and inverse-Fourier transforms, together with time-domain gating for clutter reduction [81]. Although Fourier-based methods can improve computational efficiency, their accuracy depends on spatial sampling, spectral coverage, and the propagation model. Li et al. demonstrated that propagation-path and wavefront-curvature errors can cause defocusing and target-position errors in through-wall tomographic SAR imaging [42].

5.4. Holographic Imaging

Holographic microwave imaging uses coherent measurements of EM field amplitude and phase to reconstruct the spatial distribution of scattering objects. In near-field imaging, the reconstruction model must account for the measurement geometry, wavefront curvature, and propagation through the wall.

Heydari and Amineh investigated near-field holographic TWRI using wideband measurements and wall-dependent PSFs. Their method reconstructed images using candidate wall thicknesses and applied structural similarity (SSIM) across frequency-subset reconstructions to estimate the wall thickness. Numerical simulations and experimental measurements through wooden walls demonstrated the proposed approach [16]. A related computational imaging technique was investigated by García-Fernández et al., who used frequency-diverse antenna radiation patterns to encode spatial information and reconstruct targets behind a wall using a single measurement channel [32]. The performance of these methods depends on the accuracy of the propagation model, measurement geometry, and system calibration. Wall-parameter estimation is discussed further in Section 7.

5.5. Diffraction Tomography

Diffraction tomography (DT) reconstructs the spatial distribution of EM contrast from measured scattered fields. Under the first-order Born approximation, the scattered field is linearly related to the contrast, allowing efficient reconstruction using Fourier-domain processing. Zhang and Hoorfar developed a 3D through-wall DT algorithm using a layered-medium Green function and inverse fast Fourier transform (IFFT) [2]. In earlier work, they also investigated a polarimetric extension using a layered-medium dyadic Green's function.

The main limitation of DT is its dependence on the weak-scattering approximation, which may not adequately represent multiple scattering from strongly contrasting targets. Limited aperture coverage can also restrict the spatial information available for reconstruction. Nonlinear inverse-scattering methods provide an alternative by considering more complete EM interactions, although they generally require more complex numerical solutions [27]. These approaches are discussed in the following subsection.

5.6. Inverse Scattering Methods

Inverse-scattering methods reconstruct the spatial distribution of EM contrast by comparing measured fields with predictions from a forward model. These methods may use linearized scattering approximations or nonlinear formulations that account for interactions between the fields and the targets. A general regularized inverse problem can be expressed as

$$\widehat{\boldsymbol{\chi}} = \arg\min_{\boldsymbol{\chi}} \left[\|\mathbf{y} - \mathcal{F}_w(\boldsymbol{\chi})\|_2^2 + \lambda \mathcal{R}(\boldsymbol{\chi}) \right], \tag{4}$$

where $\mathbf{y}$ represents the measurements, $\mathcal{F}_w$ is the wall-aware forward operator, $\boldsymbol{\chi}$ is the unknown contrast, λ is the regularization parameter, and $\mathcal{R}$ is the regularization function. This equation represents a general formulation rather than a particular published implementation [10,27].

Soldovieri and Solimene investigated linear inverse scattering using the Born approximation and truncated singular-value decomposition (TSVD) [10]. Song et al. developed a nonlinear 2D inversion method for multilayered environments and demonstrated its performance using multifrequency numerical data [82]. Three-dimensional microwave building tomography has also been investigated [83].

Fedeli et al. developed a wall-aware nonlinear inverse-scattering method using layered-medium Green's functions and Lebesgue-space regularization, with preliminary numerical validation [27]. Randazzo et al. subsequently introduced a two-step variable-exponent regularization approach guided by an initial delay-and-sum image and experimentally evaluated metallic and low-contrast targets behind a brick wall [84].

Figure 6 illustrates the effect of regularization on the reconstruction of a simulated dielectric target. Although nonlinear inverse scattering can account for more complex EM interactions, it generally requires greater computational effort and depends on the accuracy of the forward model.

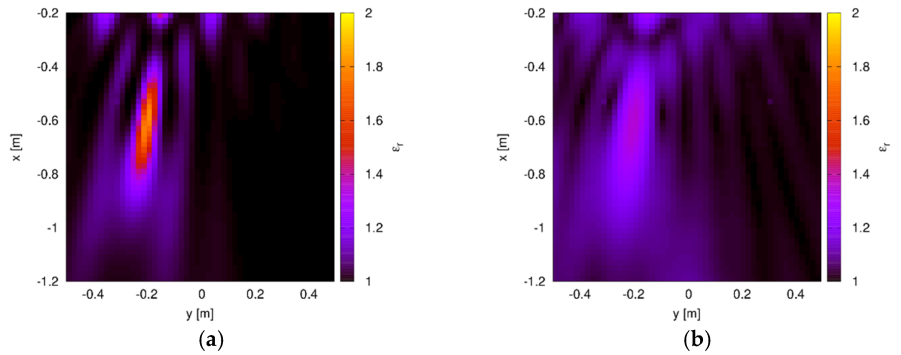


Figure 6. Numerical reconstruction of a dielectric cylinder behind a wall using (**a**) optimized Lebesgue-space regularization ($p = 1.3$) and (**b**) conventional Hilbert-space regularization ($p = 2$). Reproduced from original Figure 5 of Fedeli et al. [27], Sensors (2020), under the Creative Commons Attribution 4.0 license (CC BY 4.0). The original figure concerns simulated through-wall measurements.

The main algorithmic limitations of inverse-scattering methods arise from their physical assumptions, regularization, and computational requirements. Linear inverse-scattering methods commonly rely on the Born approximation, which may become inaccurate for

strongly scattering targets or when multiple scattering is significant [10,82]. Furthermore, inverse-scattering problems are often ill-posed, making reconstruction sensitive to noise, incomplete measurements, and the choice of regularization [10,27]. Although regularization improves solution stability, strong regularization may suppress useful target details [27,84]. Nonlinear inverse-scattering methods can account for more complex EM interactions, but they generally require repeated forward calculations and greater computational effort [27,82]. Therefore, reconstruction accuracy depends not only on the quality of the acquired measurements but also on the validity of the EM forward model and the selected inversion method.

5.7. Sparse and Compressive Imaging

Sparse and compressive imaging methods assume that the scene, or a suitable representation of it, contains only a limited number of significant coefficients. Under this assumption, useful reconstructions may be obtained from fewer frequency samples, antenna positions, or channels than in conventional full-data imaging. A representative formulation is

$$\hat{\mathbf{x}} = \arg\min_{\mathbf{x}} \left\{ \frac{1}{2} \|\mathbf{y} - \mathbf{A}\mathbf{x}\|_2^2 + \lambda \|\mathbf{x}\|_1 \right\}, \tag{5}$$

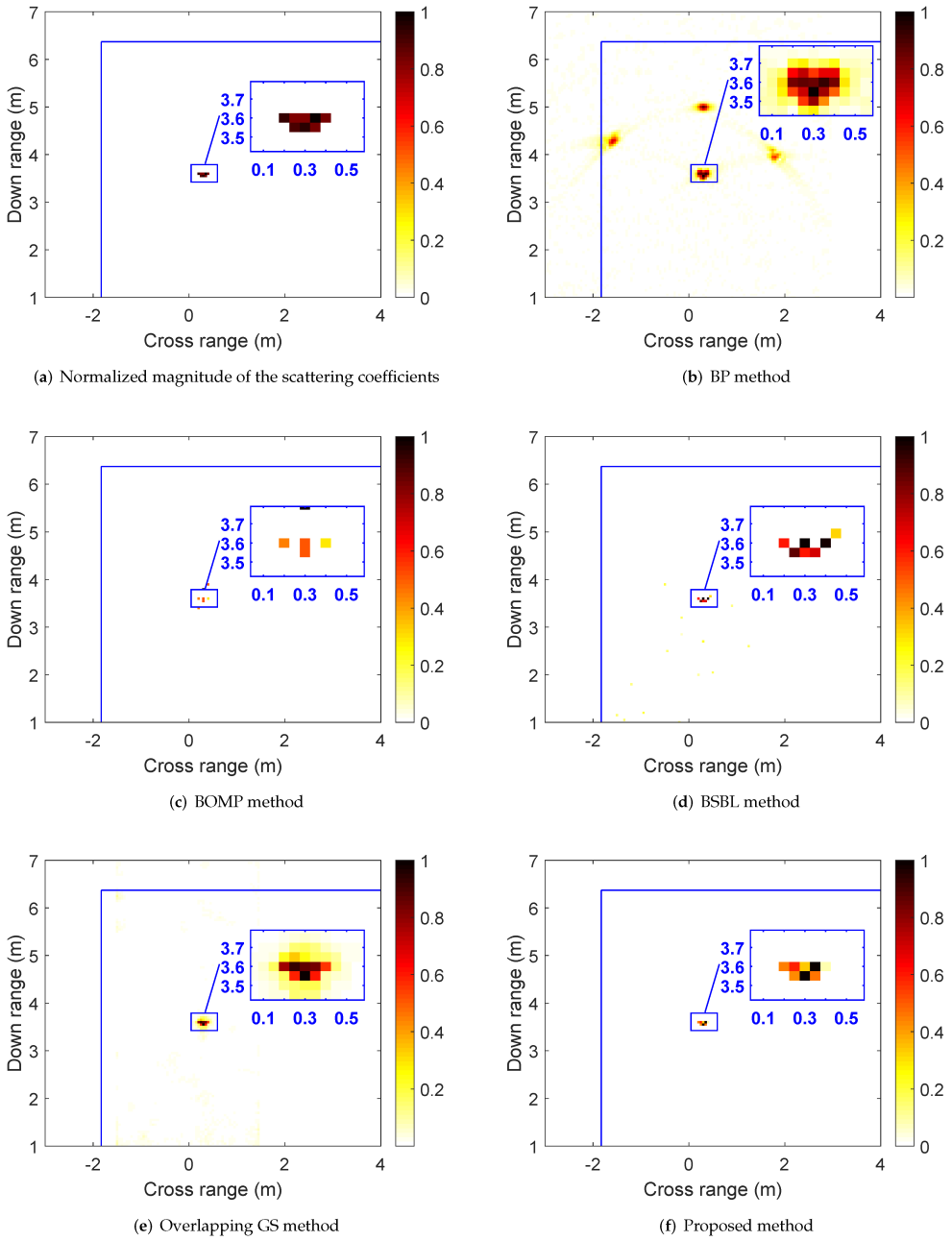
where $\mathbf{A}$ is the sensing matrix, $\mathbf{x}$ is the reflectivity vector, and λ controls the sparse regularization. In practice, sparse TWRI methods also use Bayesian priors, structured sparsity, and other constraints [9,11].

Zhang et al. applied compressive sensing to UWB impulse-radar TWRI with incomplete measurements [9]. Barzegar et al. extended compressed sensing to 3D TWRI [11], while Muqaibel et al. combined sparse reconstruction with an aperture design intended to separate true target responses from aspect-dependent artifacts [68]. These studies show that reduced measurement count does not automatically imply proportional reductions in acquisition time or computational cost.

Because many targets are spatially extended, several studies adopted structured sparse models rather than simple pixel sparsity. Wang et al. proposed a two-level block matching pursuit method for polarimetric TWRI, using clustered support and shared sparsity across polarization channels [85]. Wu et al. developed a multitask Bayesian model with shared support across subbands and multipath modes [86]. Xu and Wu later introduced a hierarchical Bayesian approach for clustered scatterers and demonstrated improved reconstruction under limited observations [49]. Related formulations have also incorporated low-rank and jointly sparse constraints for multipolarization data [14] and Bayesian models for clustered targets with multipath [12].

Figure 7 compares conventional backprojection and different sparse reconstruction methods for a simulated through-wall radar scene. The results illustrate how structured sparsity can improve target reconstruction and suppress unwanted responses when the available measurements are limited [49]. However, differences in measurement sampling between the compared methods should be considered when interpreting their performance.

Sparse and regularized reconstruction methods have also been investigated for through-wall imaging using wireless communication signals. Depatla et al. [70] combined Wi-Fi power measurements with sparse reconstruction to recover hidden structures. Karanam and Mostofi [71] investigated 3D through-wall imaging using Wi-Fi measurements collected by unmanned aerial vehicles. Guo et al. [72] used reweighted total variation regularization to improve building layout reconstruction from radio tomographic measurements.



(**a**) Normalized magnitude of the scattering coefficients (**b**) BP method

(**c**) BOMP method (**d**) BSBL method

(**e**) Overlapping GS method (**f**) Proposed method

Figure 7. Comparison of through-wall radar image reconstruction methods for a simulated scene: (**a**) normalized magnitude of the scattering coefficients (reference target distribution); (**b**) back-projection (BP) method; (**c**) block orthogonal matching pursuit (BOMP) method; (**d**) block sparse Bayesian learning (BSBL) method; (**e**) overlapping group sparsity (GS) method; and (**f**) proposed reconstruction method. Reproduced from Figure 3 of Xu and Wu [49], Applied Sciences (2022), under the CC BY 4.0 license.

Despite their advantages, sparse reconstruction methods may become unreliable when the investigated scene does not satisfy the assumed sparsity model. Conventional pixel-wise sparsity is more suitable for isolated scatterers, while extended targets and continuous structures may occupy many image pixels. Enforcing excessive sparsity in such cases can suppress weaker scattering regions, fragment object boundaries, or retain only the strongest scattering points. Structured and clustered sparsity can partly address these limitations by incorporating relationships between neighboring scattering responses [12,49]. However, these approaches still depend on the suitability of the assumed target structure. In heterogeneous or multilayered wall environments, inaccurate propagation models can introduce

dictionary mismatch, potentially causing false responses, defocusing, and localization errors [35,40]. Furthermore, when distributed scattering occupies a large portion of the reconstruction domain, the sparsity assumption may no longer support reliable recovery from highly reduced measurements. These limitations highlight the importance of appropriate scene representations and accurate EM forward models.

5.8. Learning-Based and Physics-Informed Image Reconstruction

Learning-based methods have received increasing attention in TWRI because they can learn relationships between measured radar signals, reconstructed images, and target distributions. Unlike conventional reconstruction algorithms, which mainly rely on specified propagation models and signal processing operations, neural networks use training data to learn useful image features. These methods have been investigated for improving spatial resolution, suppressing artifacts, reconstructing target shapes, and estimating unknown wall properties. However, their performance depends on the available training data and the similarity between the training and measurement conditions.

Convolutional neural networks (CNNs) are among the most widely investigated learning-based approaches. Qu et al. [87] proposed a multiresolution fusion network based on deep layer aggregation to enhance through-the-wall radar images in complex indoor environments containing scatterers with different reflection strengths. Their method combines features at different resolutions to improve the localization of weaker scattering objects while suppressing sidelobes and ghost artifacts. The effectiveness of the proposed approach was demonstrated using both simulated and experimental radar data. Zeng et al. [88] introduced a less-forgetting high-resolution network (LFHRNet) to address the limited availability of labeled through-wall radar images. Their method uses pretrained network knowledge and parallel learning branches to improve image reconstruction when only a small target-domain dataset is available. These studies illustrate the potential of CNN-based models for image enhancement, although the reconstructed details remain dependent on the learned training distribution.

Generative adversarial networks (GANs) have also been investigated for reducing image artifacts. Jia et al. [20] proposed a GAN-based method that learns a mapping between radar images containing multipath ghosts and corresponding images with reduced ghost responses. Their simulation results demonstrated the potential of learned image correction without explicitly estimating every multipath propagation path. However, the dependence on simulated training examples limits the conclusions that can be drawn about performance in unknown real environments. Figure 8 illustrates the conditional GAN framework investigated by Jia et al. [20], in which a generator and discriminator are trained to suppress multipath artifacts in reconstructed radar images. The corresponding imaging results are presented in Figure 9. The comparison shows that the GAN-based method reduces unwanted multipath responses while preserving the main target locations in the investigated simulated scenes. However, further experimental validation is required to evaluate its performance under different wall materials and acquisition conditions.

Transformer-based methods provide another approach by modeling relationships among image features over larger spatial regions. Zhong et al. [89] developed CWSNet, which combines convolutional feature extraction with transformer-based graph reasoning to reconstruct building layouts from wall and corner information. The method was evaluated using simulated and experimental datasets. In a related application, Yang et al. [38] proposed multimodal fusion using a transformer to estimate spatially varying wall parameters in complex building structures. Although the latter method focuses on wall characterization rather than direct target reconstruction, it provides information that can support propagation compensation. Ghorbani and Soleimani [90] also investigated simultaneous

estimation of wall and object parameters using a deep neural network, illustrating how learned models can support both scene characterization and wall-property estimation.

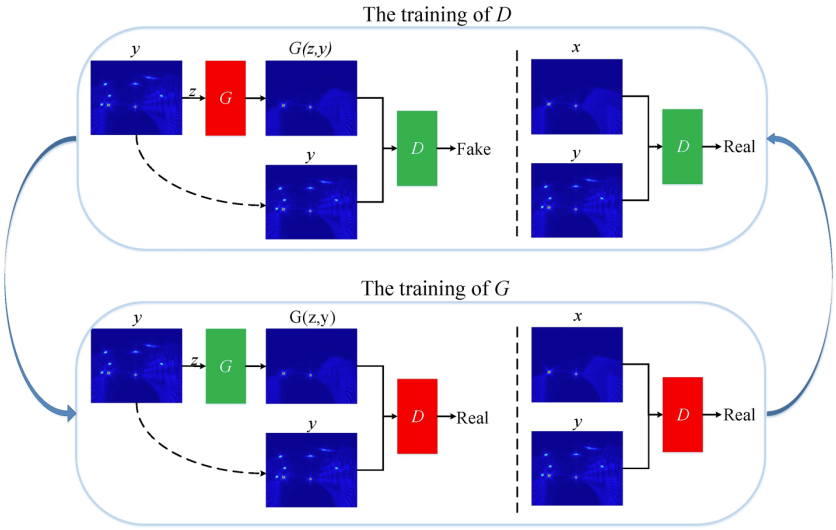


Figure 8. Training framework of a conditional generative adversarial network for suppressing multi-path artifacts in through-the-wall radar images. Reproduced from Figure 2 of Jia et al. [20], under the CC BY 4.0 license.

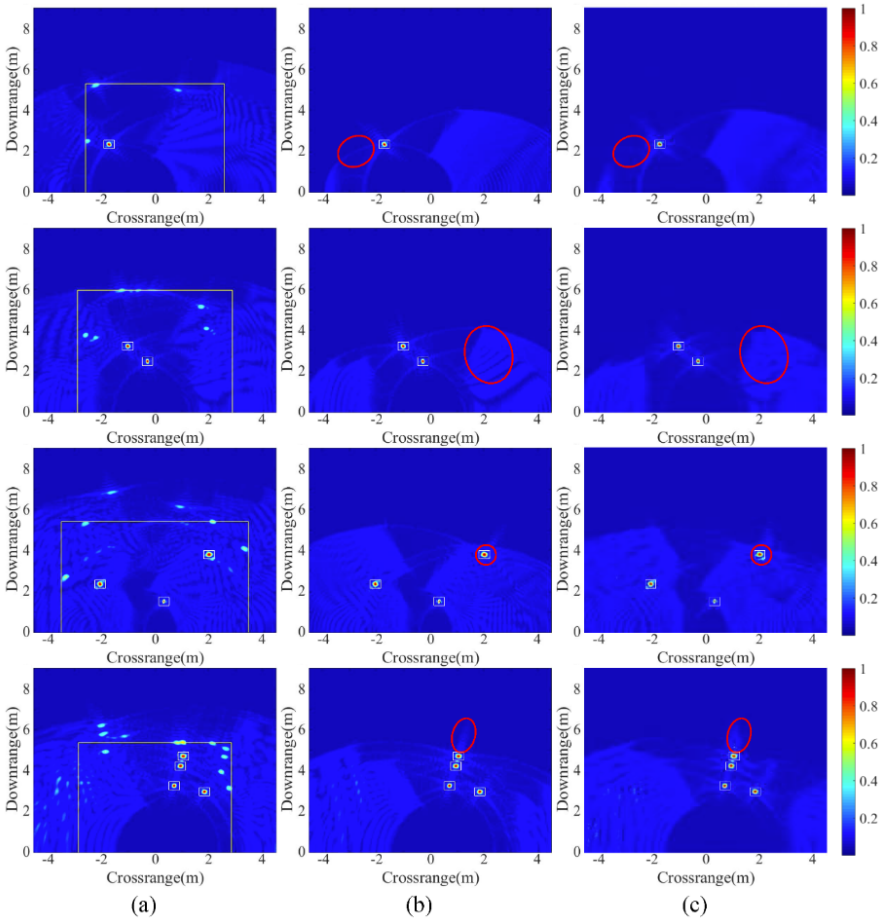


Figure 9. Comparison of simulated through-the-wall radar images before and after GAN-based multipath artifact suppression: (**a**) input images containing multipath ghosts; (**b**) reference images; and (**c**) reconstructed images after GAN processing. Reproduced from Figure 7 of Jia et al. [20], under the CC BY 4.0 license.

Diffusion models have recently been introduced for learning the distribution of radar images and progressively generating improved reconstructions. Zeng et al. [91] investigated diffusion-based super-resolution imaging for through-wall sensing, extending learning-based reconstruction beyond conventional CNN and GAN approaches. Unlike a single-pass image enhancement network, a diffusion model uses a sequence of denoising operations to generate an image consistent with its learned representation. Such methods are promising for recovering image details from limited-resolution measurements. Nevertheless, visually improved images do not necessarily represent physically correct target structures, and measurement consistency must be assessed before interpreting generated details as actual scatterers.

An important development is the combination of neural networks with EM propagation models. Wang et al. [92] proposed CS-Net, a physical model-driven deep network for TWRI. The method combines a learned CNN prior with a data-consistency operation derived from the radar measurement model and converts iterative compressed-sensing reconstruction into a trainable network. Simulation results showed improvements over the conventional compressed-sensing method under the investigated conditions. This approach preserves a direct relationship between the predicted image and measured radar data while allowing network parameters to be learned.

Physics-informed neural networks (PINNs) extend this idea by introducing governing equations and physical constraints into network training. Li et al. [93] developed a Maxwell-equation-informed framework for reconstructing irregular dielectric targets from near-field measurements. Aziz and Alipour [94] also investigated PINNs for estimating dielectric-property distributions from sparse radar measurements, including experimental multilayered-material scenarios. These studies are relevant to TWRI because wall transmission and target scattering are governed by the same EM principles. However, they should be regarded as related inverse-scattering developments rather than direct demonstrations of complete through-wall image reconstruction.

Overall, learning-based TWRI can be divided into data-driven image enhancement and reconstruction, learned wall characterization, and physics–data dual-driven inversion. Purely data-driven models can improve image quality but may be sensitive to changes in wall materials, target distributions, acquisition geometries, and noise conditions. Physics-guided models introduce measurement consistency or EM constraints that can reduce the dependence on image statistics alone.

To provide a systematic comparison of the reconstruction methods discussed in this section, Table 4 summarizes their characteristics in terms of spatial resolution, sidelobe suppression, computational requirements, sampling conditions, localization accuracy, noise robustness, sensitivity to wall parameters, applicable target structures, and reference measurement requirements.

Table 4. Evidence-based qualitative comparison of through-the-wall radar image reconstruction methods. The characteristics are conditional on measurement configuration, model assumptions, and implementation.

Method/Sources	Resolution	Sidelobe/ Artifact Control	Computational Cost	Sampling Needs	Localization Accuracy	Noise Robustness	Wall Sensitivity	Target Structures	Reference Data
DAS beamforming [1,28,81]	Bandwidth- and aperture-limited PSF	Windowing/ coherence weighting can suppress artifacts	Direct summation; cost grows with image grid	Sufficient frequency and aperture coverage	Depends on modeled travel times	Coherent integration; no general robustness guarantee	Errors in wall delays lead to defocusing	Point-like and extended reflectors	Empty-scene scan not inherent; may be used for clutter removal
Backprojection [26,48,81]	Limited by bandwidth, aperture, and viewing geometry	Coherence weighting/ filtering available	Pixel-wise accumulation; acceleration possible	Flexible antenna geometry if known	Wall-aware delays improve focus and position	Depends on SNR and preprocessing	Strong sensitivity when propagation delays are mismatched	Point-like and extended reflectors	Background and direct-coupling subtraction reported in [26]
Diffraction tomography [2,11]	Limited by measured spatial-frequency support/ Born model	Spectral filtering; residual artifacts possible	Efficient FFT/IFFT implementation	Angular/ frequency coverage; CS variants allow reduction	Good with adequate wall Green's function	Evaluated with measurement and noise-contaminated data; no universal rank	Layered-medium model important	Objects adequately represented by linearized scattering	Empty-scene subtraction used in reported studies [2,11]
Linear inverse scatter-ing/TSVD [10]	Controlled by singular-value spectrum and coverage	Truncation trades detail for stability	SVD-based; operator-size-dependent	Informative frequencies and views	Model- and regularization-dependent	Stability motivated by regularized inversion	Known wall layer in the studied formulation	Weak and strong scatterers examined; Born approximation remains a limitation	No intrinsic empty-scene requirement established
Nonlinear inverse scattering [27,82,84]	Distributed contrast reconstruction possible	Iterative regularization suppresses unstable components	Repeated nonlinear forward/inverse solves	Informative multifrequency and viewing data	Can recover position, shape, material contrast under appropriate conditions	Ill-posed; depends on regularization and noise	Accurate layered-media representation needed	Extended dielectric objects/material distributions	Calibration or background information setup-dependent

Table 4. *Cont.*

Method/Sources	Resolution	Sidelobe/ Artifact Control	Computational Cost	Sampling Needs	Localization Accuracy	Noise Robustness	Wall Sensitivity	Target Structures	Reference Data
Near-field holography [3,16]	Depends on near-field aperture, bandwidth, and PSF	PSF quality/focusing determine artifacts	FFT-based variants can be efficient	Spatially sampled near-field field measurements	Propagation or PSF mismatch can shift/blur image	SNR-dependent; no standardized cross-study rank	Sensitive to wall/PSF mismatch	Reflecting objects and spatially extended features	Experimental calibration/background strategy is implementation-specific
Sparse/ compressive imaging [11,12,49,85]	Fine localization for compatible sparse/structured scenes	Sparse and grouped priors suppress unwanted responses	Iterative; Bayesian sampling can be expensive	Reduced data possible when sensing assumptions hold	Sensitive to dictionary/support mismatch	Evaluated under selected noise levels; prior-dependent	Wall and multipath dictionary mismatch important	Sparse, clustered, or jointly sparse scene representations	Empty-scene subtraction used in some implementations, e.g., [11]
Data-driven neural imaging [20,87,88,91]	Learned sharpening; not proof of physical resolution gain	CNN/GAN-based artifact suppression studied	Training costly; inference architecture-dependent	Training-compatible inputs and representative data	Generalization to new target/wall distributions uncertain	Training and test noise distributions matter	Domain shift across walls may degrade performance	Structures sufficiently represented in training	Paired training labels common; Qu et al. used background subtraction
Physics-guided neural imaging [92–94]	Depends on measurement model and learned priors	Measurement consistency/equation constraints	Unrolled or constrained iterative optimization	Measurement coverage and model fidelity matter	Dependent on forward-model accuracy	Not directly comparable across included studies	Model mismatch remains a limitation	TWRI reflectivity; related dielectric inverse-scattering examples	Training or calibration requirements vary; some cited PINNs are not direct TWRI demonstrations

6. Wall and Background Clutter Mitigation

Strong unwanted reflections are a major obstacle to TWRI. The front wall can return considerably more energy than objects behind it, while antenna coupling, wall reverberation, and other stationary scatterers add further unwanted responses. When these components are not sufficiently reduced, a weak target may be hidden even when a suitable image reconstruction algorithm is used [13,15]. Clutter mitigation therefore aims to reduce unwanted responses while preserving the spatial and phase information required for image formation. This task is different from wall compensation, which corrects propagation-related errors, and from multipath processing, which addresses indirect propagation paths. Those problems are considered in Sections 7 and 8, respectively.

6.1. Sources of Clutter in TWRI

For radar measurements collected at different antenna positions and frequencies, the received data can be represented by a simplified additive model [15]:

$$\mathbf{D} = \mathbf{W} + \mathbf{T} + \mathbf{B} + \mathbf{N}, \tag{6}$$

where $\mathbf{D}$ represents the measured data, $\mathbf{W}$ denotes wall reflections and reverberation, $\mathbf{T}$ contains the desired target responses, $\mathbf{B}$ represents other background clutter, and $\mathbf{N}$ denotes measurement noise. This decomposition is conceptual, as the individual contributions may overlap and cannot always be separated exactly. Wall reflections can persist over long delay intervals and obscure weaker targets [13]. Additional clutter may arise from direct antenna coupling and scattering by background objects [15]. In reinforced walls, reflections from steel rebars can resemble target echoes in radar B-scans, complicating clutter suppression [95].

Wall echoes are often spatially similar across a linear aperture parallel to a relatively uniform wall, whereas returns from a localized target vary more strongly with antenna position. This difference motivates spatial filtering and subspace methods [13]. It is less reliable for nonuniform or nonplanar walls, irregular acquisition geometries, and extended targets. Lagunas et al. specifically considered heterogeneous walls whose frequency- and position-dependent responses undermine simple spatial-invariance assumptions [40].

Direct antenna coupling and wall reverberation may both appear in the early-time portion of the received signal, making their separation challenging. One approach is to measure the direct coupling response separately using a calibration measurement without the wall and targets. For example, Hu et al. [26] measured direct antenna coupling by directing the antenna array toward an open area and subtracting the recorded response from the measured data. In a related near-field holographic microwave imaging study, Heydari and Amineh [3] used microwave-absorbing materials to reduce antenna coupling and applied no-object reference responses for measurement compensation. However, when direct coupling and wall echoes overlap in time, simple time gating cannot reliably separate them. Background subtraction may reduce both contributions without identifying them individually. Therefore, their separation depends on suitable calibration measurements and stable measurement conditions.

6.2. Background and Reference Subtraction

Background subtraction uses a reference measurement of the same scene without the target. The processed data are obtained by subtracting the reference response from the measured data:

$$\mathbf{D}_{\mathrm{BS}} = \mathbf{D} - \mathbf{D}_{\mathrm{ref}}. \tag{7}$$

where $\mathbf{D}_{\mathrm{ref}}$ is the complex reference measurement. When the wall, radar position, and measurement conditions remain unchanged, this operation can suppress a large portion of the

wall and static-background responses. Yoon and Amin used background subtraction as a reference for evaluating spatial filtering methods and reported comparable imaging results under their experimental conditions [13]. However, background subtraction requires a target-free reference measurement, which may not be available in practical TWRI scenarios.

The main limitation is the availability and stability of the reference data. In an unknown building, obtaining an empty-scene measurement may be impossible. Changes in antenna position, calibration, or the environment can also leave subtraction residuals, even if the wall itself is unchanged [15]. Thus, background subtraction is most suitable for controlled measurements or scenes in which reference acquisitions are possible, rather than being a general solution for unknown occupied rooms.

6.3. Spatial Filtering, Mean Subtraction, and Differential Processing

Mean subtraction estimates the component common to measurements along the aperture and removes it from each spatial trace. Following the principle of spatial wall-clutter filtering discussed by Yoon and Amin [13], a representative mean-subtraction operation can be expressed as

$$\tilde{d}_n(f) = d_n(f) - \frac{1}{N}\sum_{q=1}^{N} d_q(f), \tag{8}$$

where $d_n(f)$ is the measurement at antenna position n and frequency f, and N is the total number of antenna positions. This operation suppresses components that change little across antenna positions. More general spatial notch filters attenuate zero and low spatial-frequency components associated with nearly invariant wall returns. Yoon and Amin tested these methods on solid, multilayered, and cinder-block walls and reconstructed images after preprocessing [13]. Spatial filtering requires neither an empty scene nor an explicit estimate of wall thickness or permittivity.

The method is sensitive to how the wall is viewed. A rough or heterogeneous wall may generate returns that vary along the aperture and therefore survive the filter, while a spatially broad or weakly varying target response may be removed together with clutter [40]. Related spatial-difference processing forms signals from adjacent antenna positions before imaging. Dehmollaian et al. demonstrated differential SAR imaging through a concrete wall, together with an integration step to compensate for changes caused to the target response by differencing [96]. This is a spatial operation, not temporal background subtraction. Neither operation should be assumed to preserve all targets without distortion.

6.4. Subspace-Based Methods: SVD and PCA

Subspace-based methods exploit differences between wall and target responses in the measured radar data. Singular value decomposition (SVD) factorizes the measurement matrix as

$$\mathbf{D} = \mathbf{U}\mathbf{\Sigma}\mathbf{V}^{H}, \tag{9}$$

where $\mathbf{U}$ and $\mathbf{V}$ contain singular vectors and $\mathbf{\Sigma}$ contains the singular values. The dominant wall-related components can be identified and suppressed through orthogonal subspace projection. Tivive et al. demonstrated that both wall and target responses may occupy multidimensional subspaces and developed an SVD-based clutter removal method using simulated and experimental data [97].

A main challenge is distinguishing wall-related components from target information, since their subspaces can overlap [97]. Eltrass combined principal component analysis (PCA) and independent component analysis (ICA) with autofocus backprojection to improve target imaging in cluttered environments [98]. These approaches do not require target-free reference measurements, but their performance depends on selecting suitable subspace components and separation criteria.

6.5. Low-Rank and Sparse Decomposition

Low-rank and sparse decomposition methods separate wall clutter from target responses by assuming that wall reflections form a low-rank component, while target information is represented by a sparse component. A common robust principal component analysis (RPCA) model is $\mathbf{D} = \mathbf{L} + \mathbf{S} + \mathbf{E}$, where $\mathbf{L}$ represents clutter, $\mathbf{S}$ represents target responses, and $\mathbf{E}$ denotes residual errors. In the noise-free case, principal component pursuit is formulated as [99]

$$\min_{\mathbf{L},\mathbf{S}} \|\mathbf{L}\|_* + \lambda\|\mathbf{S}\|_1 \quad \text{subject to} \quad \mathbf{D} = \mathbf{L} + \mathbf{S}, \tag{10}$$

where $\|\cdot\|_*$ is the nuclear norm and λ controls the balance between the two components.

Tang et al. combined low-rank clutter suppression with jointly sparse polarimetric reconstruction [14]. Liu et al. applied a two-stage RPCA method after backprojection and demonstrated improved target visibility using simulated and experimental data [15]. Brehier et al. introduced Kronecker-structured RPCA with robust loss functions to address heterogeneous noise and outliers [45]. Chen et al. investigated low-rank and sparse separation using ADMM [100], while Zhang et al. combined range-migration compensation with low-rank and sparse decomposition to suppress rebar clutter [95]. Tivive and Bouzerdoum also investigated a sparse-autoencoder approach with low-rank projection [101].

These methods can reduce wall clutter without requiring target-free reference measurements. However, their effectiveness depends on the assumed low-rank and sparse structure, which may not fully represent heterogeneous walls or extended targets.

Bivalkar et al. investigated entropy-based low-rank approximation for TWRI of targets with different dielectric properties [102]. Figure 10 presents experimental B-scan examples, illustrating the effect of low-rank processing on target visibility.

6.6. Temporal Filtering and Change-Based Methods

Temporal filtering uses measurements collected at different times to suppress stationary background responses and emphasize changes associated with moving targets. Through-wall SAR imaging of vibrating targets has been investigated using simulated and experimental measurements [56], although this study does not directly evaluate temporal clutter subtraction.

A limitation of temporal subtraction is that stationary targets may also be removed with the background. Time-domain gating is a different approach that suppresses returns within selected delay intervals, but it may remove nearby target responses or fail to eliminate delayed wall reverberation.

6.7. Model-Based Mitigation and Comparative Assessment

Model-based clutter mitigation estimates wall reflections and subtracts them from the measured data without necessarily requiring an empty-scene reference. Lagunas et al. estimated wall-reflection amplitude and delay for heterogeneous walls and subtracted the modeled response before sparse reconstruction [40]. However, the performance of this approach depends on the accuracy of the wall model.

Other approaches suppress clutter in the image domain. Yang et al. proposed amplitude-coherence-factor weighting for MIMO TWRI and evaluated the method using simulated and experimental data [44]. Unlike measurement-domain subtraction, this method attenuates image pixels according to their across-channel amplitude statistics.

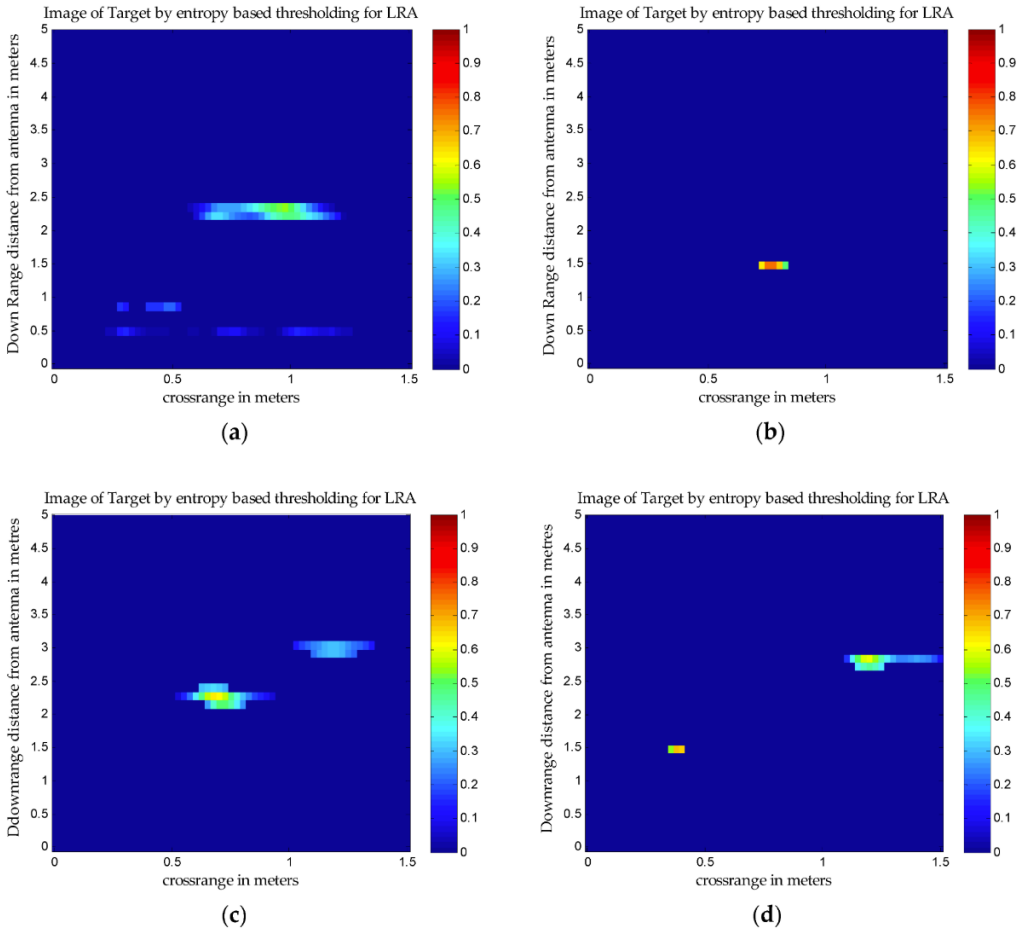


Figure 10. Experimental through-wall radar B-scan images reconstructed using entropy-based low-rank approximation: (**a**) a single metal target; (**b**) a single wooden target; (**c**) two metal targets; and (**d**) a metal target and a wooden target. The color bars represent normalized image intensity. Source: Bivalkar et al. [102], original Figure 6(a–d), Electronics 2019, *8*, 634 (CC BY 4.0).

Table 5 summarizes the main advantages and limitations of the clutter-mitigation approaches discussed in this section. Their effectiveness depends on wall properties, acquisition geometry, and target characteristics. Therefore, comparisons should consider both clutter suppression and target preservation under consistent evaluation conditions.

Table 5. Comparison of representative wall-clutter mitigation methods in TWRI. Advantages and limitations depend on the acquisition conditions, wall properties, and target characteristics.

Method	Main Principle	Advantages	Limitations	References
Background subtraction	Subtract target-free reference measurements	Simple implementation and effective suppression under stable conditions	Requires a target-free reference and stable measurement conditions	[13]
Spatial filtering	Remove spatially invariant or slowly varying wall responses	Low computational cost; no reference measurements required	May suppress extended targets or retain spatially varying wall clutter	[13]

Table 5. *Cont.*

Method	Main Principle	Advantages	Limitations	References
Differential SAR	Subtract measurements at adjacent antenna positions	Suppresses correlated wall reflections without explicit wall parameters	May distort target responses and require additional correction	[96]
SVD/PCA and ICA	Identify and suppress clutter-related data components	Data-adaptive; does not require target-free measurements	Component selection and overlap between wall and target subspaces	[97,98]
Low-rank and sparse decomposition	Separate correlated clutter and sparse target responses	Can combine clutter suppression with image reconstruction	Depends on structural assumptions; iterative processing may be costly	[14,45]
Parametric wall modeling	Estimate and subtract wall reflections using a propagation model	Can handle spatially varying clutter without target-free data	Sensitive to modeling errors and unmodeled reflections	[40]
Image-domain coherence weighting	Attenuate wall-related image responses using channel statistics	Can improve target visibility in suitable MIMO configurations	Depends on channel diversity and the selected weighting criterion	[44]

7. Wall Compensation and Wall-Parameter Uncertainty

The wall changes the travel time, direction, phase, and amplitude of radar signals passing between the antennas and a target. If image reconstruction assumes free-space propagation, these changes can shift target responses away from their actual positions and reduce image focus [1,80]. Wall compensation accounts for these propagation effects in the imaging model. Unlike the clutter suppression methods discussed in Section 6, its main purpose is not to remove the strong wall echo but to correct the propagation paths used to reconstruct objects behind the wall. This section reviews compensation with known wall properties, the effects of parameter uncertainty, and methods for estimating the properties needed for reliable imaging.

7.1. Imaging with Known Wall Parameters

When wall thickness and EM properties are known, the imaging algorithm can calculate the propagation path through the wall instead of treating the complete path as free space. A basic model represents the wall as a dielectric slab with known thickness and relative permittivity. Wall-aware synthetic aperture beamforming uses the refraction and additional delay introduced by this slab to focus signals from behind-wall targets [1]. Dehmollaian and Sarabandi examined image distortion caused by building walls and demonstrated refocusing using a matched response based on the assumed wall characteristics [80]. These studies show why propagation compensation must be included before target position and shape are interpreted from the reconstructed image.

Wall compensation can be introduced into different reconstruction algorithms. For DAS or backprojection imaging, the free-space delay is replaced with a travel time calculated for the air–wall–air path [1]. For diffraction tomography and inverse scattering, the forward model can include transmission through the dielectric slab and use the appropriate Green function for the layered medium [10,27]. Such approaches account for the wall during image formation rather than trying to correct the completed image afterward. Jin and Yarovoy also examined TWRI using a more realistic propagation model, emphasizing the role of physical modeling in the reconstruction process [66].

A single homogeneous slab is not sufficient for every building structure. Zhang and Hoorfar extended 3D synthetic aperture imaging to multilayered walls, where propagation depends on the properties and thicknesses of the individual layers [6]. For more complicated geometries, Watson et al. used a full-wave description of transmission and scattering by the obscuring structure within a multistatic synthetic aperture framework [35]. These richer models can represent effects that are omitted by a simple delay correction, but they also require more information about the wall and can increase the computational cost. Consequently, the choice of compensation model involves a balance between physical accuracy, available prior knowledge, and processing requirements.

7.2. Effects of Incorrect Wall Parameters

Accurate compensation depends on the parameters supplied to the propagation model. The most frequently considered quantities are wall thickness d and relative permittivity ε_r; conductivity and loss may also matter when attenuation and frequency-dependent transmission are modeled [5,27]. If thickness or permittivity is incorrect, the calculated travel time and phase no longer match the measured signals. As a result, reconstructed targets can appear displaced in range, spread across neighboring pixels, or less sharply focused [17,80].

Wall-parameter errors do not necessarily affect every target in the same way. Their influence also depends on antenna position, incidence angle, and the location of the target relative to the wall. Wang and Amin analyzed these position-dependent shifts and used the differences between images formed at multiple stand-off distances to resolve wall ambiguity [103]. Errors can become more difficult to correct when several wall layers contribute different propagation delays and transmission effects [6].

Thickness and permittivity are also coupled in the measured propagation delay. For example, under a simplified normally incident, low-loss slab model, the additional one-way delay relative to the same distance in air is approximately $d(\sqrt{\varepsilon_r}-1)/c_0$, where c_0 is the free-space wave speed. Thus, different combinations of thickness and permittivity can produce similar delays. Additional information, such as angle-dependent measurements, front- and rear-surface reflections, or measurements at multiple radar positions, may be needed to distinguish these parameters [17,103]. This coupling is important when interpreting an estimated parameter pair: a focused image does not, by itself, guarantee that each wall property has been recovered uniquely.

Wall thickness and relative permittivity are coupled through the propagation delay. For a homogeneous, low-loss wall under normal incidence, the additional two-way propagation phase relative to the corresponding air path can be approximated as [103]

$$\Delta\phi = \frac{4\pi f d}{c_0}(\sqrt{\varepsilon_r}-1). \tag{11}$$

Applying a first-order Taylor expansion gives the following approximation for small errors in wall thickness and relative permittivity:

$$\delta\phi \approx \frac{4\pi f}{c_0}\left[(\sqrt{\varepsilon_r}-1)\delta d + \frac{d}{2\sqrt{\varepsilon_r}}\delta\varepsilon_r\right]. \tag{12}$$

This relationship illustrates the coupling between wall thickness and permittivity, which can introduce ambiguities in wall-parameter estimation and affect image focusing and target localization [17,103]. The resulting phase mismatch can reduce coherent focusing and introduce image defocusing and target-position errors [1]. Additional observations, such as multiple viewing angles, measurements at different stand-off distances, or wall-interface reflections, can provide information to reduce this ambiguity [104].

7.3. Wall-Parameter Estimation from Radar Measurements

One approach is to estimate wall properties from the measured radar signals before reconstructing the target scene. For a relatively simple wall, the reflections from its front and rear surfaces contain information about wall thickness and propagation speed. Solimene et al. proposed a two-step method in which the early portion of the measured field is used to estimate slab parameters, followed by 3D imaging using a linear inverse scattering procedure [17]. Using the early-time wall response reduces the influence of later target returns in the parameter-estimation step, although separation becomes more difficult when the relevant echoes overlap.

Other methods use differences between acquisition positions rather than relying only on the wall-interface echoes. Wang and Amin formed images using different stand-off distances and related the resulting target displacement trajectories to candidate wall properties [103]. Their approach uses the fact that an incorrect wall model causes position errors that change with the observation geometry. For distributed radar arrangements, Yao et al. used consistency of the target states observed by different radar nodes to estimate wall thickness, while assuming prior knowledge of the dielectric constant [43]. Their later work considered simultaneous target localization and wall-parameter estimation using target-position consistency, multipath relationships, and fusion between distributed radar measurements [33]. These methods provide additional geometric constraints but depend on reliable relationships between observations of the same target.

In distributed TWRI, different radar nodes may observe different multipath reflections because their positions and surrounding geometries differ. These reflections can produce ghost responses and affect target localization [19,21]. Therefore, target-state consistency does not require identical received signals at all radar nodes. Instead, the estimated positions of the same target should agree after accounting for radar geometry and wall-induced propagation effects [43]. Yao et al. [33] combined wall compensation with target-position consistency and used relationships among multipath, targets, and walls to support parameter estimation. However, when multipath reflections are incorrectly identified as direct target responses, the estimated target positions may become inconsistent [21]. Multipath-aware reconstruction methods can help account for indirect propagation paths when suitable models are available [12,19]. Nevertheless, maintaining target consistency remains challenging when the room geometry is unknown or several reflection paths overlap. Therefore, reliable target association and accurate propagation models are important for distributed radar imaging.

Wall estimation becomes more challenging when the material properties change across the wall. Yasmeen and Ram proposed GAN-based inversion to estimate dielectric profiles for homogeneous walls, layered walls, and walls containing air gaps; they also evaluated the method using measurements of physical walls [36]. Such approaches can represent a spatial distribution of properties rather than one effective permittivity for the complete barrier. However, their predictions depend on the range of wall structures, radar configurations, and measurement conditions represented during model development. Estimated wall properties are useful for imaging only when they can be incorporated into a compatible propagation model.

7.4. Autofocusing Approaches

Autofocusing estimates unknown wall parameters by examining the quality of reconstructed images. Instead of measuring the wall properties separately, the algorithm

reconstructs images using different candidate parameters and selects the values that produce the preferred image-quality measure. In a general form, this process can be written as

$$\hat{\boldsymbol{\theta}} = \arg\max_{\boldsymbol{\theta}\in\Theta} Q(I(\boldsymbol{\theta})), \tag{13}$$

where $\boldsymbol{\theta}$ contains the unknown wall parameters, Θ is their candidate range, $I(\boldsymbol{\theta})$ is the reconstructed image, and Q is a focusing criterion. A metric defined as a cost rather than a quality score would instead be minimized. Autofocusing is attractive when direct measurements of wall thickness or material properties are unavailable, but its result depends on the selected criterion and the range of candidate parameters.

Ahmad et al. developed an autofocusing method based on image contrast expressed through standardized higher-order statistics, demonstrating that wall characteristics can be adjusted to improve the focus of through-wall imagery [104]. Dehmollaian and Sarabandi also used image-domain optimization to estimate wall characteristics and refocus synthetic aperture images [80]. These methods connect parameter estimation directly to reconstruction quality, but a high-contrast image may still contain artifacts or incorrectly positioned targets if the propagation model or the metric is unsuitable.

The main computational difficulty is the repeated evaluation of candidate wall parameters. Searching over both thickness and permittivity may require many reconstructions. Jin et al. proposed echo-domain and image-domain filtering approaches for this problem and showed that image-domain filtering avoids repeating the complete image-formation operation during every adjustment; they also reduced the search dimension to improve efficiency [105]. Singh and Singh subsequently proposed a method that evaluates a selected subset of thickness–permittivity combinations rather than an exhaustive parameter grid, with experimental validation of the reduced computation [18]. In a related hybrid approach, they combined compressive measurements with a direct estimate of wall permittivity and then performed autofocus over wall thickness, reducing the number of parameters searched during image formation [106].

7.5. Joint Wall and Scene Estimation

The preceding methods often estimate the wall first and then reconstruct the scene. A different formulation treats wall properties and scene information as related unknowns. This is important because an incorrect wall model can make the reconstructed target distribution appear wrong, while an inaccurate scene estimate can also affect the inferred wall properties. A joint approach therefore updates or predicts both groups of unknowns, rather than keeping one fixed throughout the reconstruction.

An alternative is to measure agreement between independently reconstructed images rather than the sharpness of one image. In near-field holographic through-wall imaging, Heydari and Amineh investigated wall-thickness estimation using a structural-similarity-based criterion applied to reconstructions from different frequency subsets [16]. This image-consistency idea is distinct from maximizing image contrast, because it compares the stability of reconstructed structure across subsets of the measurements. It should not be treated as generally more accurate than conventional autofocus without comparisons under matched conditions. For all image-based methods, noise, residual wall clutter, target geometry, and incorrect forward models can change the optimum of the focusing criterion.

Watson et al. formulated multistatic through-wall imaging with unknown wall properties as an inverse problem in which the wall parameters act as nuisance parameters coupled to the target reflectivity [35]. Their approach uses a more complete transmission model and reduced-order representations to make repeated forward calculations more practical. The reported demonstrations included an unknown wall permittivity in two-dimensional image reconstruction, while broader geometry estimation and fully vectorial EM modeling

remained outside the demonstrated cases [35]. Compared with simple autofocus, this framework accounts more directly for agreement between predicted and measured radar data, at the cost of more complicated modeling and optimization.

Learning-based methods provide another form of coupled estimation. Ghorbani and Soleimani trained a deep neural network to predict wall thickness and permittivity together with target position and target permittivity for scenes containing one or two targets [90]. However, this represents simultaneous parameter prediction rather than the general reconstruction of an arbitrary reflectivity image. Its usefulness for image formation depends on whether the predicted parameters remain accurate for walls and target arrangements outside the training cases. The distributed-radar method of Yao et al. also combines wall compensation with target localization, using the agreement of target positions across radar nodes to support parameter estimation [33]. These examples show that joint estimation can use physical inversion, learned mappings, or geometric consistency, but the types of estimated scene information are not identical across methods.

7.6. Compensation for Complex and Nonuniform Walls

Many reported compensation and autofocus techniques begin with a uniform, planar wall. Actual building structures may contain several materials, air gaps, internal reinforcement, doors, windows, or changes in thickness. Under these conditions, one average thickness and permittivity may not describe the propagation paths across the complete antenna aperture. Multilayer imaging methods address part of this problem by representing each layer separately [6]. Other models allow the obscuring structure to have more general geometry and include transmission effects beyond those captured by a planar-slab approximation [35].

Recent work has also investigated spatially varying wall properties. Yasmeen and Ram used learned inversion to recover dielectric profiles for several inhomogeneous wall arrangements [36]. Yang et al. proposed a multimodal framework that combines optical and LiDAR-based geometry information with radar measurements to estimate wall parameters for separate wall segments and assemble a spatial parameter map [38]. Zeng et al. investigated multifrequency fusion imaging for nonuniform wall scenarios, addressing the need for reconstruction methods that do not rely entirely on a single uniform-wall description [39]. These directions are relevant to image compensation because the propagation correction can vary with the antenna position and the portion of the wall crossed by each path.

Table 6 compares the principal approaches. The literature indicates that more detailed wall models can improve the physical consistency of image formation, but only when their parameters can be estimated with sufficient reliability. For practical TWRI, an important unresolved issue is how to obtain accurate wall information without requiring extensive measurements, a large parameter search, or training data covering every possible building structure. Equally important is separating image-focus improvements from actual improvements in target position and shape accuracy. Future comparisons should therefore report wall-estimation error, localization error, image-quality measures, computational cost, and performance under realistic wall variability using clearly defined evaluation conditions.

Table 6. Comparison of approaches for wall compensation and wall-parameter uncertainty in TWRI. The limitations are qualitative and do not imply a numerical ranking across studies.

Approach	Main Principle and Representative Work	Main Limitation
Known-wall compensation	Use wall-aware travel times, transmission models, or layered Green's functions [1,6].	Requires sufficiently accurate wall geometry and material properties.
Direct echo-based estimation	Estimate wall properties from early-time reflections, then reconstruct targets [17].	Interface echoes may overlap or be weak.
Geometric or multiview estimation	Enforce consistent target positions across observation geometries [33,103].	Requires suitable viewing diversity and reliable target correspondence.
Image autofocusing	Optimize a focus measure over candidate wall parameters [18,104,105].	Repeated reconstructions can be costly; the best focus need not imply unique parameters.
Joint wall–scene estimation	Couple wall properties with target reflectivity or target parameters [35,90].	More unknowns increase the need for constraints, data, or training coverage.
Spatially varying estimation	Recover local wall profiles or segment-wise property maps [36,38].	Requires richer measurements or representative training data.

8. Multipath Processing in TWRI

Multipath propagation is one of the major challenges in TWRI, as indirect reflections can introduce false targets and degrade image reconstruction quality. However, these additional reflections may also provide useful information that can improve imaging performance when properly modeled. This section discusses the formation of multipath artifacts, reviews methods for their mitigation, and examines approaches that exploit multipath information to enhance target reconstruction.

8.1. Multipath Propagation and Ghost Formation

In TWRI, the received signals may contain both direct and indirect reflections from targets. Direct returns follow the expected propagation path between the radar and a target, whereas multipath returns involve additional reflections from surrounding walls, floors, ceilings, or other objects. When an imaging algorithm interprets these indirect returns as direct reflections, they may appear at incorrect locations and produce false targets, commonly called multipath ghosts [19,20]. Unlike the strong front-wall reflections discussed in Section 6, multipath signals may depend on the presence and location of the targets themselves. Therefore, removing stationary wall clutter does not necessarily eliminate multipath artifacts.

The formation of multipath ghosts depends on the geometry of the environment, the antenna configuration, and the propagation paths. In addition to reflections involving interior walls, EM waves may scatter between multiple targets, producing interaction multipath. Ma et al. investigated this effect and showed that target-to-target interactions can introduce additional ghost responses, particularly in scenes containing several closely located scatterers [107]. Multipath processing consequently requires either distinguishing indirect returns from direct responses or incorporating the additional propagation paths into the imaging model.

8.2. Multipath Mitigation Methods

Multipath mitigation aims to reduce false responses while preserving the reconstructed images of actual targets. One approach is to use a propagation model that accounts for the differences between direct and indirect signal paths. Ma et al. proposed a compressive sensing (CS) method that includes target-to-target interaction multipath in the reconstruction dictionary. Their simulations with five to eight point targets showed improved ghost suppression compared with conventional CS under the evaluated conditions [107]. However, the method requires a more complicated signal model and was evaluated using simulated scenes.

Other approaches use the spatial properties of multipath signals rather than explicitly modeling every reflection path. Zhu et al. developed a two-step method for MIMO TWRI that combines group-sparse reconstruction with spatial filtering based on the directions of departure and arrival. Their simulation results demonstrated the potential to separate direct target responses from multipath components [108]. More recently, Liao et al. proposed virtual array rotation to exploit the dependence of ghost locations on observation geometry. Their method combines phase compensation, cross-correlation backprojection, and image fusion to suppress ghosts without requiring prior knowledge of the indoor layout. Both numerical simulations and measured data were used for validation [109].

Learning-based approaches have also been investigated for removing multipath artifacts from reconstructed images. Jia et al. developed a GAN that learns to transform images containing multipath ghosts into images with reduced ghost responses [20]. This approach does not require explicit identification of every multipath propagation path during image correction. However, its effectiveness depends on the training data, and the reported evaluation was primarily based on generated radar images. Generalization to different wall materials, room geometries, and measurement conditions therefore remains an important consideration.

8.3. Multipath Exploitation for Improved Imaging

Although multipath propagation can degrade image quality, indirect reflections also contain information about the targets and their surrounding environment. Instead of suppressing these signals, multipath exploitation methods attempt to associate them with their corresponding targets and use them to strengthen reconstruction. Wu et al. combined a modified Green function with backprojection to identify multipath responses and map their contributions toward the locations of actual targets. Their numerical and experimental results demonstrated improved target visibility and reduced ghost interference under the investigated conditions [19].

Multipath information has also been incorporated into sparse reconstruction frameworks. Wu et al. developed a Bayesian compressive sensing approach that exploits both multipath information and the spatial structure of targets, allowing these properties to contribute jointly to image recovery [12]. Mkemwa et al. further investigated multipath-aware path-loss compensation and clutter isolation to improve the reconstruction of targets affected by propagation losses. Their work included numerical and experimental evaluation [46].

These studies show that multipath is not always an unwanted component of radar measurements. Suppression methods are useful when indirect returns introduce strong artifacts, whereas exploitation methods can provide additional information when the relevant propagation paths are sufficiently well modeled. However, exploitation may become unreliable when the room geometry or reflection characteristics are unknown. A key research challenge is therefore to develop imaging algorithms that distinguish useful multipath contributions from misleading ghost responses without requiring detailed prior knowledge of the environment. Future comparisons should evaluate ghost suppression, target

preservation, localization accuracy, and computational cost using consistent numerical and experimental conditions.

9. Image-Based Target Localization and Quantitative Performance Evaluation

The usefulness of a through-the-wall radar image depends on whether the reconstructed responses represent the positions and spatial extent of the actual targets. A visually sharp image is not necessarily accurate: wall-induced focusing errors, sidelobes, and multipath may produce strong responses at incorrect locations. This section considers target localization from reconstructed images and the quantitative evidence needed to evaluate imaging performance.

9.1. Target Localization from Reconstructed Images

For an isolated, compact target, a simple localization estimate is the position of a prominent image-intensity peak. For an extended target, the position may instead be estimated from the centroid or intensity-weighted center of a selected image region. These choices do not always produce the same result, because the strongest radar response may arise from only one part of an object. Moreover, weak targets may be obscured by nearby sidelobes or false responses. Xu and Wu showed that explicitly considering the clustered structure of target pixels can improve the recovery of spatially extended responses and reduce isolated artifacts in their evaluated through-wall scenes [49].

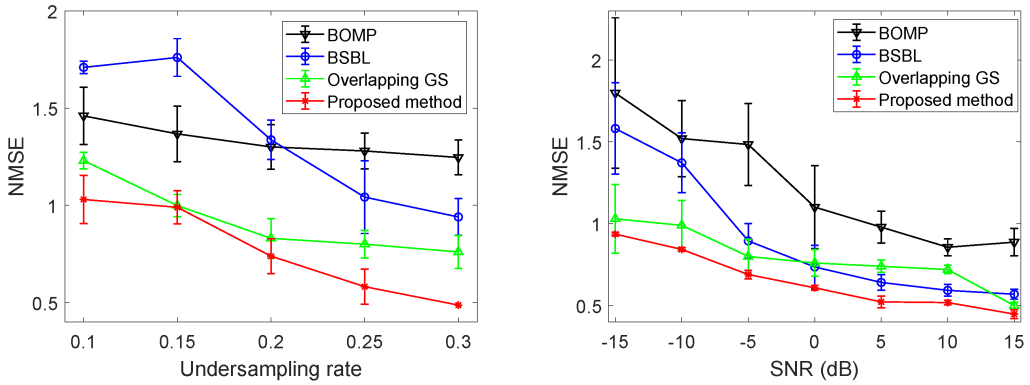
Localization also depends on the propagation model used to form the image. Incorrect wall parameters may shift the reconstructed target response, even if the target remains clearly visible. Liao et al. investigated propagation compensation and coherence-based weighting for 3D MIMO imaging [41]. Li et al. analyzed path-related and wavefront-curvature errors in through-wall tomographic SAR, illustrating additional sources of defocusing and position error [42]. Distributed observations can provide complementary position constraints: Yao et al. combined target localization with wall-parameter estimation and fused estimates from multiple radar views, validating their approach with simulations and measurements [33]. Thus, localization should be evaluated against independently known target positions, rather than inferred only from image brightness.

9.2. Quantitative Image Quality and Localization Metrics

The basic meanings of resolution, SNR, SCR, contrast, and localization error were introduced in Section 3 and are summarized in Table 1. Their practical use requires consistent definitions and evaluation regions. For a target with estimated position $\hat{\mathbf{r}}$ and reference position $\mathbf{r}_{\mathrm{ref}}$, localization error can be reported as $e_{\mathrm{loc}} = \|\hat{\mathbf{r}} - \mathbf{r}_{\mathrm{ref}}\|_2$. For multiple targets, an evaluation should also specify how estimated responses are associated with reference targets and how missed targets and false peaks are handled. These details help distinguish a small position error from merely obtaining a strong-looking image.

Image-wide measures provide complementary information when a suitable reference image or known target distribution is available. Normalized mean square error (NMSE) expresses reconstruction differences after a stated normalization, while structural similarity (SSIM) emphasizes agreement in image structure. Xu and Wu evaluated their structure-aware Bayesian imaging method under different measurement sampling rates and noise levels, reporting NMSE curves for several reconstruction algorithms [49]. Zeng et al. used SSIM with reference images to assess the effect of wall compensation on reconstructed building layouts [37]. Such measures answer different questions; lower reconstruction error, greater contrast, or a sharper image does not by itself establish better target localization.

Figure 11 illustrates how a quantitative ranking depends on data availability and noise. Xu and Wu examined undersampling rates from 10% to 30% and SNR values from −15 to 15 dB; their proposed method generally obtained lower NMSE than the compared sparse reconstruction methods in these simulated conditions [49]. These results demonstrate sensitivity to acquisition conditions, but they should not be read as a direct measurement of localization error or as a universal performance ranking across different walls and imaging systems.



(**a**) NMSE versus undersampling rate (**b**) NMSE versus SNR

Figure 11. Comparison of normalized mean square error (NMSE) for simulated through-the-wall radar reconstruction methods: (**a**) variation with the measurement undersampling rate and (**b**) variation with the signal-to-noise ratio (SNR). Reproduced from original Figure 4 of Xu and Wu [49], Applied Sciences (2022), under CC BY 4.0.

9.3. Performance Comparison and Evaluation Challenges

Direct numerical comparisons across TWRI publications are difficult when the radar configurations and test scenes differ. Effective bandwidth, aperture sampling, target distance, wall material, and reconstruction grid all influence image quality. For example, Pisa et al. experimentally compared different array configurations and reported trade-offs between acquisition time and cross-range resolution [7]. Maisto et al. analyzed how the arrangement of measurement positions affects the sampled PSF [30]. Performance differences between papers therefore cannot be assigned to reconstruction algorithms alone unless these acquisition factors are controlled.

The strength of validation evidence is another important factor when evaluating TWRI methods. Existing studies can be classified into three levels: simulation-only validation, controlled laboratory experiments, and field measurements in real buildings. Simulations demonstrate algorithm performance under assumed conditions, while laboratory experiments evaluate performance using physical walls and measured radar data. Field measurements provide stronger evidence of practical applicability by including more realistic wall structures, clutter, and environmental variations. However, successful results in simulations or controlled experiments do not necessarily guarantee reliable imaging in real buildings. Table 7 summarizes these validation levels and their limitations.

Table 7 distinguishes three levels of validation reported in TWRI research. Simulation studies demonstrate reconstruction performance under known conditions, while laboratory experiments provide evidence using physical walls and measured radar data. Real-building experiments provide additional evidence of practical applicability. For example, Le et al. [110] reconstructed the interior layout of an actual building using measurements from different sides, while Li et al. [111] evaluated imaging artifact suppression using a vehicle-mounted radar scanning a building. Nevertheless, successful field measurements do not guarantee reliable performance in all buildings. Further validation under different

wall materials, geometries, and environmental conditions remains necessary. The type of validation is equally important. Simulated scenes provide known target positions and reference images, whereas measured scenes introduce calibration errors, nonuniform walls, uncertain scattering behavior, and limited ground truth. Computational cost should also be considered alongside reconstruction quality. In the experiments reported by Xu and Wu, the proposed method required more processing time than the simpler BOMP baseline, despite achieving lower NMSE in their simulation [49]. Future evaluations would be more informative if they reported acquisition settings, wall assumptions, target-location errors, image-quality metrics, and runtime under clearly specified conditions. Whenever possible, the same measured dataset and reference positions should be used to compare competing methods, with both target preservation and false-response suppression assessed.

Table 7. Comparison of validation evidence in TWRI studies. The levels describe experimental conditions and do not represent universal rankings of algorithm performance.

Level	Conditions	Representative Studies	Evidence	Limitations
Level 1: Simulation	Numerical models with assumed wall, target, and noise conditions	[1,27,82]	Algorithm feasibility under known conditions	Does not establish measured-data performance or robustness in real buildings
Level 2: Laboratory	Physical walls and controlled radar measurement configurations	[2,16,26,49]	Practical image reconstruction under tested experimental conditions	Limited wall and target variability; calibration and reference measurements may influence results
Level 3: Field	Measurements of actual building structures using deployed radar systems	[110,111]	Building-scale imaging and experimentally validated artifact suppression	Results remain site- and method-specific; generalization is not established

When comparing TWRI reconstruction methods, hardware and acquisition limitations should be distinguished from algorithmic constraints. In particular, reconstruction errors may arise from insufficient measurement information or from inaccurate physical assumptions and numerical approximations, and these sources of error should be evaluated separately.

10. Conclusions

This paper reviewed the main methods used for through-the-wall radar image reconstruction, wall-clutter mitigation, wall compensation, and multipath processing. The comparison showed that reconstruction performance depends on several connected factors, including the available radar measurements, acquisition geometry, wall properties, propagation model accuracy, and target characteristics. Conventional beamforming and back-projection provide relatively straightforward image formation, while inverse scattering, diffraction tomography, holography, sparse reconstruction, and learning-based methods offer additional capabilities under different assumptions. However, each approach introduces trade-offs involving image quality, computational complexity, measurement requirements, and model sensitivity.

One important finding is that wall-clutter mitigation and wall compensation address different imaging problems. Clutter mitigation reduces unwanted wall and background reflections, whereas wall compensation corrects propagation-related errors that can cause defocusing and incorrect target localization. Therefore, improving target visibility does not necessarily imply an improvement in geometric accuracy. The review also highlighted the coupling between wall thickness and relative permittivity of the unknown wall, which can make wall-parameter estimation ambiguous. Advanced estimation and compensation methods can reduce these errors, but their effectiveness depends on the available information and the accuracy of the assumed propagation model.

Multipath processing presents another important trade-off. Indirect reflections may produce false target responses when interpreted as direct propagation paths. However, when the relevant paths can be identified and modeled, multipath signals may also contribute useful information for target reconstruction. Similarly, sparse and learning-based techniques can improve image quality under suitable conditions, but their performance depends on assumptions about target structure, training data, and measurement consistency.

The reviewed literature also shows that direct performance comparisons remain difficult because studies use different wall materials, antenna configurations, imaging geometries, target scenes, and evaluation metrics. Numerical simulations and controlled laboratory experiments provide valuable evidence, but they do not fully establish the performance of these methods in real buildings. Future studies may report reconstruction accuracy, target localization error, clutter and ghost suppression, computational cost, and sensitivity to wall-parameter uncertainty under clearly defined conditions.

Future research should prioritize robust and computationally efficient reconstruction through complex, nonuniform, and multilayered walls; joint estimation of wall parameters and target distributions; and integrated clutter and multipath processing. Efficient 3D imaging and the combination of physics-based EM propagation models with learning-based techniques are also promising directions. Further improvements in modeling target structures are needed to support the reconstruction of large objects and distributed scatterers. In addition, measurements in realistic buildings and more consistent evaluation procedures are necessary to assess the general applicability of emerging imaging methods. Addressing these challenges will help improve the accuracy, reliability, and practical applicability of TWRI systems.

Author Contributions: Conceptualization, M.H. and R.K.A.; writing—original draft preparation, M.H.; writing—review and editing, R.K.A.; supervision, R.K.A. All authors have read and agreed to the published version of the manuscript.

Funding: This research received no external funding.

Institutional Review Board Statement: Not applicable.

Informed Consent Statement: Not applicable.

Data Availability Statement: No new data were created or analyzed in this study. Data sharing is not applicable to this article.

Conflicts of Interest: The authors declare no conflicts of interest.

References

1. Ahmad, F.; Amin, M.G.; Kassam, S.A. Synthetic aperture beamformer for imaging through a dielectric wall. *IEEE Trans. Aerosp. Electron. Syst.* **2005**, *41*, 271–283. [CrossRef]
2. Zhang, W.; Hoorfar, A. 3D real-time through-the-wall radar imaging with diffraction tomographic algorithm. *IEEE Trans. Geosci. Remote Sens.* **2013**, *51*, 4155–4163. [CrossRef]
3. Heydari, M.; Amineh, R.K. Expedited Near-Field Holographic Microwave Imaging with an Azimuthally Distributed Antenna Array. *Electronics* **2025**, *14*, 2518. [CrossRef]
4. Heydari, M.; Amineh, R.K. Fast Near-Field Holographic Microwave Imaging with a Novel Data Acquisition Technique. In *Proceedings of the 2026 IEEE International Symposium on Antennas and Propagation and USNC-URSI Radio Science Meeting (AP-S/USNC-URSI), Detroit, MI, USA, 12–17 July 2026*; IEEE: New York, NY, USA, 2026; pp. 504–507. [CrossRef]
5. Muqaibel, A.H.; Alsunaidi, M.A.; Iya, N.M.; Safaai-Jazi, A. Wall attenuation and dispersion. In *Through-the-Wall Radar Imaging*; Amin, M.G., Ed.; CRC Press: Boca Raton, FL, USA, 2011; pp. 1–32.
6. Zhang, W.; Hoorfar, A. 3D synthetic aperture radar imaging through multilayered walls. *IEEE Trans. Antennas Propag.* **2014**, *62*, 459–462. [CrossRef]
7. Pisa, S.; Cicchetti, R.; Piuzzi, E.; Testa, O. A comparison between multiple-input multiple-output and multiple-input single-output radar configurations for through-the-wall imaging applications. *Int. J. Antennas Propag.* **2022**, *2022*, 3887314. [CrossRef]
8. Paun, M. Through-wall imaging using low-cost frequency-modulated continuous wave radar sensors. *Remote Sens.* **2024**, *16*, 1426. [CrossRef]
9. Zhang, W.; Amin, M.G.; Ahmad, F.; Hoorfar, A.; Smith, G.E. Ultrawideband impulse radar through-the-wall imaging with compressive sensing. *Int. J. Antennas Propag.* **2012**, *2012*, 251497. [CrossRef]
10. Soldovieri, F.; Solimene, R. Through-wall imaging via a linear inverse scattering algorithm. *IEEE Geosci. Remote Sens. Lett.* **2007**, *4*, 513–517. [CrossRef]
11. Salehi Barzegar, A.; Cheldavi, A.; Sedighy, S.H.; Nayyeri, V. 3-D through-the-wall radar imaging using compressed sensing. *IEEE Geosci. Remote Sens. Lett.* **2022**, *19*, 3504805. [CrossRef]
12. Wu, Q.; Lai, Z.; Amin, M.G. Through-the-wall radar imaging based on Bayesian compressive sensing exploiting multipath and target structure. *IEEE Trans. Comput. Imaging* **2021**, *7*, 422–435. [CrossRef]
13. Yoon, Y.-S.; Amin, M.G. Spatial filtering for wall-clutter mitigation in through-the-wall radar imaging. *IEEE Trans. Geosci. Remote Sens.* **2009**, *47*, 3192–3208. [CrossRef]
14. Tang, V.H.; Bouzerdoum, A.; Phung, S.L. Multipolarization through-wall radar imaging using low-rank and jointly-sparse representations. *IEEE Trans. Image Process.* **2018**, *27*, 1763–1776. [CrossRef] [PubMed]
15. Liu, L.; Chen, Q.; Han, Y.; Xu, H.; Li, J.; Wang, B. Improved clutter removal by robust principal component analysis for chaos through-wall imaging radar. *Electronics* **2020**, *9*, 25. [CrossRef]
16. Heydari, M.; Amineh, R.K. Near-field holographic through-the-wall imaging with wall thickness estimation. In *Proceedings of the 2026 IEEE International Symposium on Antennas and Propagation and USNC-URSI Radio Science Meeting (AP-S/URSI), Detroit, MI, USA, 12–17 July 2026*; IEEE: New York, NY, USA, 2026 ; pp. 512–515. [CrossRef]
17. Solimene, R.; Soldovieri, F.; Prisco, G.; Pierri, R. 3D through-wall imaging under ambiguous wall parameters. *IEEE Trans. Geosci. Remote Sens.* **2009**, *47*, 1310–1317. [CrossRef]
18. Singh, A.P.; Singh, V. An efficient autofocusing technique for through-the-wall radar imaging. *IEEE Sens. Lett.* **2025**, *9*, 3506704. [CrossRef]
19. Wu, S.; Zhou, H.; Liu, S.; Duan, R. Improved through-wall radar imaging using modified Green's function-based multi-path exploitation method. *EURASIP J. Adv. Signal Process.* **2020**, *2020*, 4. [CrossRef]
20. Jia, Y.; Song, R.; Chen, S.; Wang, G.; Guo, Y.; Zhong, X.; Cui, G. Multipath ghost suppression based on generative adversarial nets in through-wall radar imaging. *Electronics* **2019**, *8*, 626. [CrossRef]
21. Abdalla, A.T.; Alkhodary, M.T.; Muqaibel, A.H. Multipath ghosts in through-the-wall radar imaging: Challenges and solutions. *ETRI J.* **2018**, *40*, 376–388. [CrossRef]
22. Nkwari, P.K.M.; Sinha, S.; Ferreira, H.C. Through-the-wall radar imaging: A review. *IETE Tech. Rev.* **2018**, *35*, 631–639. [CrossRef]
23. Abdalla, A.T. Through-the-wall radar imaging with compressive sensing; theory, practice and future trends—A review. *Tanzan. J. Sci.* **2018**, *44*, 12–30. [CrossRef]
24. Kileo, A.; Iddi, H.U.; Abdalla, A. Fast sparse image reconstruction models in through-the-wall radars: A review. *Tanzan. J. Sci.* **2026**, *52*, 19. [CrossRef]
25. Edgar, T.; Ally, A.F.; Abdalla, A.T. Leveraging Convolutional Neural Networks for Through-the-Wall Radar Imaging: Challenges, Impacts, and Future Directions. *Tanzan. J. Eng. Technol.* **2026**, *45*, 1–11. Available online: https://commons.udsm.ac.tz/tjet/vol45/iss1/1/ (accessed on 11 November 2026).
26. Hu, Z.; Zeng, Z.; Wang, K.; Feng, W.; Zhang, J.; Lu, Q.; Kang, X. Design and analysis of a UWB MIMO radar system with miniaturized Vivaldi antenna for through-wall imaging. *Remote Sens.* **2019**, *11*, 1867. [CrossRef]

27. Fedeli, A.; Pastorino, M.; Ponti, C.; Randazzo, A.; Schettini, G. Through-the-wall microwave imaging: Forward and inverse scattering modeling. *Sensors* **2020**, *20*, 2865. [CrossRef] [PubMed]
28. Ahmad, F.; Zhang, Y.; Amin, M.G. 3D wideband beamforming for imaging through a single wall. *IEEE Geosci. Remote Sens. Lett.* **2008**, *5*, 176–179. [CrossRef]
29. Zhang, W. 3D through-the-wall imaging with multiple-input multiple-output (MIMO) radar. *J. Electromagn. Waves Appl.* **2014**, *28*, 1935–1943. [CrossRef]
30. Maisto, M.A.; Masoodi, M.; Pierri, R.; Solimene, R. Sensor arrangement in through-the-wall radar imaging. *IEEE Open J. Antennas Propag.* **2022**, *3*, 333–341 . [CrossRef]
31. Li, X.; Ye, S.; Wang, Z.; Yuan, Y.; Liu, X.; Fang, G.; Ma, D. A compact stepped frequency continuous waveform through-wall radar system based on dual-channel software-defined radio. *Electronics* **2025**, *14*, 527. [CrossRef]
32. García-Fernández, M.; Àlvarez-Narciandi, G.; Yurduseven, O. Single channel frequency-diverse computational imaging system for through-the-wall sensing. *IEEE Trans. Geosci. Remote Sens.* **2024**, *62*, 5105110. [CrossRef]
33. Yao, Y.; Chen, J.; Guo, S.; Hao, X.; Li, N.; Cui, G.; Kong, L. Target localization and wall parameters estimation via distributed through-wall imaging radar. *IEEE Trans. Instrum. Meas.* **2025**, *74*, 6500611. [CrossRef]
34. Hao, X.; Chen, J.; Guo, S.; Li, N.; Yao, Y.; Qiu, C.; Cui, G. A robust multi-channel calibration method for MIMO through-the-wall radar systems. *IEEE Trans. Antennas Propag.* **2026**, *74*, 7118–7123. [CrossRef]
35. Watson, F.M.; Andre, D.; Lionheart, W.R.B. Resolving full-wave through-wall transmission effects in multi-static synthetic aperture radar. *Inverse Probl.* **2024**, *40*, 085009. [CrossRef]
36. Yasmeen, K.; Ram, S.S. Estimation of electrical characteristics of inhomogeneous walls using generative adversarial networks. *IEEE J. Sel. Top. Appl. Earth Obs. Remote Sens.* **2023**, *16*, 7009–7023. [CrossRef]
37. Zeng, X.; Hu, Y.; Yang, X.; Yin, Z.; Zhong, S. A multisource fusion system for through-wall radar compensation using LiDAR and SLAM-based 3-D reconstruction. *IEEE Sens. J.* **2025**, *25*, 29363–29377. [CrossRef]
38. Yang, X.; Wang, P.; Zeng, X.; Yin, Z.; Miao, Y. Transformer-based multi-modal fusion for complex wall parameter distribution estimation. *IEEE Internet Things J.* **2026**, *13*, 27038–27050. [CrossRef]
39. Zeng, X.; Miao, Y.; Yin, Z.; Gong, J.; Yang, X. Multifrequency fusion imaging algorithm for nonuniform wall scenarios. *IEEE Sens. J.* **2026**, *26*, 12179–12189. [CrossRef]
40. Lagunas, E.; Amin, M.G.; Ahmad, F. Through-the-wall radar imaging for heterogeneous walls using compressive sensing. In *Proceedings of the International Workshop on Compressed Sensing Theory and Its Applications to Radar, Sonar and Remote Sensing (CoSeRa)*; IEEE: New York, NY, USA, 2015. [CrossRef]
41. Liao, J.; Zeng, X.; Yang, X.; Yin, Z.; Chen, Z. MIMO through-the-wall radar 3-D imaging using propagation compensation and coherence factor. *IEEE Trans. Aerosp. Electron. Syst.* **2025**, *61*, 17213–17226. [CrossRef]
42. Li, W.; Chen, L.; Tang, H.; Zhang, F.; Xu, X.; Zhang, C.; Liu, J.; Yu, J. Error analysis and correction method of through-wall tomographic SAR. *IEEE Trans. Aerosp. Electron. Syst.* **2025**, *early access*. [CrossRef]
43. Yao, Y.; Guo, S.; Chen, J. Wall parameter estimation method based on consistent target states for distributed through-wall imaging radar. In Proceedings of the Photonics & Electromagnetics Research Symposium (PIERS), Chengdu, China, 21–25 April 2024. [CrossRef]
44. Yang, X.; Zhang, D.; Wang, Y.; Meng, H.; Qu, X. Wall clutter suppression method based on amplitude coherence factor for MIMO through-the-wall radar. *IEEE Signal Process. Lett.* **2024**, *31*, 2490–2494. [CrossRef]
45. Brehier, H.; Breloy, A.; Ren, C.; Ginolhac, G. Through the wall radar imaging via Kronecker-structured Huber-type RPCA. *Signal Process.* **2024**, *214*, 109228. [CrossRef]
46. Mkemwa, F.; Abdalla, A.T.; Maiseli, B.; Amour, I.; Muqaibel, A. Effective path-loss compensation model based on multipath exploitation for through-the-wall radar imaging. *EURASIP J. Adv. Signal Process.* **2023**, *2023*, 42. [CrossRef]
47. Debes, C.; Amin, M.G.; Zoubir, A.M. Target detection in single- and multiple-view through-the-wall radar imaging. *IEEE Trans. Geosci. Remote Sens.* **2009**, *47*, 1349–1360. [CrossRef]
48. Dass, R.; Nel, W.; Paine, S. Application of 2D and 3D SAR backprojection techniques for intrawall and throughwall object detection. In *Proceedings of the 2025 IEEE Radar Conference (RadarConf)*; IEEE: New York, NY, USA, 2025. [CrossRef]
49. Xu, C.; Wu, Q. High-resolution through-the-wall radar imaging with exploitation of target structure. *Appl. Sci.* **2022**, *12*, 11684. [CrossRef]
50. Maaref, N.; Millot, P. Array-based ultrawideband through-wall radar: Prediction and assessment of real radar abilities. *Int. J. Antennas Propag.* **2013**, *2013*, 602716. [CrossRef]
51. Narayanan, R.M.; Gebhardt, E.T.; Broderick, S.P. Through-wall single and multiple target imaging using MIMO radar. *Electronics* **2017**, *6*, 70. [CrossRef]
52. Li, Y.-C.; Oh, D.; Kim, S.; Chong, J.-W. Dual channel S-band frequency modulated continuous wave through-wall radar imaging. *Sensors* **2018**, *18*, 311. [CrossRef] [PubMed]

53. Abedi, H.; Zakeri, B. Through-the-multilayered wall imaging using passive synthetic aperture radar. *IEEE Trans. Geosci. Remote Sens.* **2019**, *57*, 4181–4191. [CrossRef]
54. Boudamouz, B.; Millot, P.; Pichot, C. Through the wall radar imaging with MIMO beamforming processing—simulation and experimental results. *Am. J. Remote Sens.* **2013**, *1*, 7–12. [CrossRef]
55. Lu, B.; Zhao, Y.; Sun, X.; Zhou, Z. Design and analysis of ultra-wideband split transmit virtual aperture array for through-the-wall imaging. *Int. J. Antennas Propag.* **2013**, *2013*, 934509. [CrossRef]
56. Corbett, B.; Andre, D.; Finnis, M. Through-wall detection and imaging of a vibrating target using synthetic aperture radar. *Electron. Lett.* **2017**, *53*, 991–995. [CrossRef]
57. Liu, J.; Jia, Y.; Kong, L.; Yang, X.; Liu, Q.H. MIMO through-wall radar 3-D imaging of a human body in different postures. *J. Electromagn. Waves Appl.* **2016**, *30*, 849–859. [CrossRef]
58. Ranjbaran, S.M.H.; Mohanna, S. Through-wall microwave imaging system using circularly polarised spiral antenna array. *IET Radar Sonar Navig.* **2019**, *13*, 937–943. [CrossRef]
59. Pan, J.; Ye, S.; Shi, C.; Yan, K.; Liu, X.; Ni, Z.; Yang, G.; Fang, G. 3D imaging of moving targets for ultra-wideband MIMO through-wall radar system. *IET Radar Sonar Navig.* **2021**, *15*, 261–273. [CrossRef]
60. Pan, J.; Liang, X.; Wu, S.; Zhao, D.; Yan, K.; Nie, J.; Hu, J.; Zhou, B.; Fang, G. 3D motion compensation method based on sparse array designed for time-division multiplexing multiple-input-multiple-output through-wall radar. *Appl. Sci.* **2023**, *13*, 8662. [CrossRef]
61. Ahmad, F.; Amin, M.G. Multi-location wideband synthetic aperture imaging for urban sensing applications. *J. Frankl. Inst.* **2008**, *345*, 618–639. [CrossRef]
62. Jia, Y.; Cui, G.; Kong, L.; Yang, X. Multichannel and multiview imaging approach to building layout determination of through-wall radar. *IEEE Geosci. Remote Sens. Lett.* **2014**, *11*, 970–974. [CrossRef]
63. Jia, Y.; Zhong, X.; Liu, J.; Guo, Y. Single-side two-location spotlight imaging for building based on MIMO through-wall-radar. *Sensors* **2016**, *16*, 1441. [CrossRef] [PubMed]
64. Seng, C.H.; Bouzerdoum, A.; Amin, M.G.; Phung, S.L. Probabilistic fuzzy image fusion approach for radar through wall sensing. *IEEE Trans. Image Process.* **2013**, *22*, 4938–4951. [CrossRef] [PubMed]
65. Chen, X.; Chen, W. Double-layer fuzzy fusion for multiview through-wall radar images. *IEEE Geosci. Remote Sens. Lett.* **2015**, *12*, 2075–2079. [CrossRef]
66. Jin, T.; Yarovoy, A. A through-the-wall radar imaging method based on a realistic model. *Int. J. Antennas Propag.* **2015**, *2015*, 539510. [CrossRef]
67. Liu, J.; Jia, Y.; Kong, L.; Yang, X.; Liu, Q.H. Sign-coherence-factor-based suppression for grating lobes in through-wall radar imaging. *IEEE Geosci. Remote Sens. Lett.* **2016**, *13*, 1681–1685. [CrossRef]
68. Muqaibel, A.H.; Abdalla, A.T.; Alkhodary, M.T.; Alawsh, S.A. Through-the-wall radar imaging exploiting Pythagorean apertures with sparse reconstruction. *Digit. Signal Process.* **2017**, *61*, 86–96. [CrossRef]
69. Zhang, W.; Hoorfar, A.; Thajudeen, C.; Ahmad, F. Full polarimetric beam-forming algorithm for through-the-wall radar imaging. *Radio Sci.* **2011**, *46*, RS0E16. [CrossRef]
70. Depatla, S.; Buckland, L.; Mostofi, Y. X-Ray Vision with Only WiFi Power Measurements Using Rytov Wave Models. *IEEE Trans. Veh. Technol.* **2015**, *64*, 1376–1387. [CrossRef]
71. Karanam, C.R.; Mostofi, Y. 3D Through-Wall Imaging with Unmanned Aerial Vehicles Using WiFi. In *Proceedings of the 16th ACM/IEEE International Conference on Information Processing in Sensor Networks (IPSN), Pittsburgh, PA, USA, 18–21 April 2017*; Association for Computing Machinery: New York, NY, USA, 2017; pp. 131–142. [CrossRef]
72. Guo, Q.; Li, Y.; Liang, X.; Dong, J.; Cheng, R. Through-the-Wall Image Reconstruction via Reweighted Total Variation and Prior Information in Radio Tomographic Imaging. *IEEE Access* **2020**, *8*, 40057–40066. [CrossRef]
73. Zhang, Y.; Chen, J.; Guo, S.; Yang, X.; Cui, G. Building Layout Tomographic Reconstruction via Commercial WiFi Signals. *IEEE Internet Things J.* **2021**, *8*, 15500–15511. [CrossRef]
74. Strohmayer, J.; Sterzinger, R.; Stippel, C.; Kampel, M. Through-Wall Imaging Based on WiFi Channel State Information. In *Proceedings of the 2024 IEEE International Conference on Image Processing (ICIP), Abu Dhabi, United Arab Emirates, 27–30 October 2024*; IEEE: New York, NY, USA, 2024; pp. 4000–4006. [CrossRef]
75. Bazzi, A.; Ying, M.; Kanhere, O.; Rappaport, T.S.; Chafii, M. ISAC Imaging by Channel State Information Using Ray Tracing for Next Generation 6G. *IEEE J. Sel. Top. Electromagn. Antennas Propag.* **2025**, *1*, 135–149. [CrossRef]
76. Li, J.; Qian, B.; Zhang, Q.; Wu, D.; Ma, D.; Huang, S.; Zhang, J.; Feng, Z. NSFNet: Neural Scattering Field Network for 3D Imaging in ISAC Systems via Multi-View CSI Fusion. *IEEE Trans. Wirel. Commun.* **2026**, *25*, 14703–14718. [CrossRef]
77. Cicchetti, R.; Pisa, S.; Piuzzi, E.; Pittella, E.; D'Atanasio, P.; Testa, O. Numerical and experimental comparison among a new hybrid FT-MUSIC technique and existing algorithms for through-the-wall radar imaging. *IEEE Trans. Microw. Theory Techn.* **2021**, *69*, 3372–3387. [CrossRef]

78. Guo, Y.; Du, N.; Zhang, G.; Liu, J.; Ye, X.; Fang, X. Robust adaptive beamforming based on physical subspace partitioning for through-wall radar imaging. In *Proceedings of the IEEE MTT-S International Microwave Workshop Series on Advanced Materials and Processes for RF and THz Applications (IMWS-AMP)*; IEEE: New York, NY, USA, 2025. [CrossRef]
79. Yang, X.; Meng, H.; Qu, X.; Gao, W. Through-the-wall radar imaging grating-lobe and sidelobe suppression method based on imaginary sign coherence factor. *IEEE Signal Process. Lett.* **2024**, *31*, 2120–2124. [CrossRef]
80. Dehmollaian, M.; Sarabandi, K. Refocusing through building walls using synthetic aperture radar. *IEEE Trans. Geosci. Remote Sens.* **2008**, *46*, 1589–1599. [CrossRef]
81. Testa, O.; Pisa, S.; Cicchetti, R. Efficient implementation of radar imaging techniques including time gating clutter removal for through the walls applications. *IEEE Access* **2025**, *13*, 63504–63518. [CrossRef]
82. Song, L.-P.; Yu, C.; Liu, Q.H. Through-wall imaging (TWI) by radar: 2-D tomographic results and analyses. *IEEE Trans. Geosci. Remote Sens.* **2005**, *43*, 2793–2798. [CrossRef]
83. Weichman, P.B.; Lavely, E.M.; Hill, E.H., III; Zemany, P.D. Through-the-wall microwave building tomography. In *Through-the-Wall Radar Imaging*; Amin, M.G., Ed.; CRC Press: Boca Raton, FL, USA, 2011; pp. 219–268.
84. Randazzo, A.; Ponti, C.; Fedeli, A.; Estatico, C.; D'Atanasio, P.; Pastorino, M.; Schettini, G. A two-step inverse-scattering technique in variable-exponent Lebesgue spaces for through-the-wall microwave imaging: Experimental results. *IEEE Trans. Geosci. Remote Sens.* **2021**, *59*, 7189–7200. [CrossRef]
85. Wang, X.; Li, G.; Liu, Y.; Amin, M.G. Two-level block matching pursuit for polarimetric through-wall radar imaging. *IEEE Trans. Geosci. Remote Sens.* **2018**, *56*, 1533–1545. [CrossRef]
86. Wu, Q.; Zhang, Y.D.; Amin, M.G.; Ahmad, F. Through-the-wall radar imaging based on modified Bayesian compressive sensing. In Proceedings of the IEEE China Summit and International Conference on Signal and Information Processing (ChinaSIP), Xi'an, China, 9–13 July 2014; pp. 232–236. [CrossRef]
87. Qu, L.; Wang, C.; Yang, T.; Zhang, L.; Sun, Y. Enhanced through-the-wall radar imaging based on deep layer aggregation. *IEEE Geosci. Remote Sens. Lett.* **2022**, *19*, 4023705. [CrossRef]
88. Zeng, X.; Zhao, H.; Zhong, S.; Yin, Z.; Yang, X. LFHRNet: Less-forgetting high-resolution network for through-wall radar imaging. *IEEE Trans. Aerosp. Electron. Syst.* **2025**, *61*, 14450–14462. [CrossRef]
89. Zhong, S.; Ma, Z.; Zeng, X.; Liu, R.; Yang, X. CWSNet: A building layout sensing network with corner and wall information fusion from through-the-wall radar. *IEEE Signal Process. Lett.* **2026**, *33*, 703–707. [CrossRef]
90. Ghorbani, F.; Soleimani, H. Simultaneous estimation of wall and object parameters in TWR using deep neural network. *Int. J. Antennas Propag.* **2022**, *2022*, 7810213. [CrossRef]
91. Zeng, X.; Chen, Z.; Yang, X.; Liao, J.; Gong, J. A diffusion model based super-resolution imaging method for through-wall sensing. *IEEE Trans. Aerosp. Electron. Syst.* **2025**, *61*, 10215–10228. [CrossRef]
92. Wang, Y.; Zhang, Y.; Xiao, M.; Zhou, H.; Liu, Q.; Gao, J. Physical model-driven deep networks for through-the-wall radar imaging. *Int. J. Microw. Wirel. Technol.* **2023**, *15*, 82–89. [CrossRef]
93. Li, H.; Liu, J.-G.; Wang, Y.; Xin, X.-D.; Huang, X.-W.; Sheng, X.-Q. Physics-informed deep learning for inverse scattering of irregular targets from near-field data. *IEEE Antennas Wirel. Propag. Lett.* **2025**, *24*, 3734–3738. [CrossRef]
94. Aziz, I.; Alipour, M. Discrete and continuous property retrieval from sparse radar observations using physics-informed neural networks. *Measurement* **2026**, *285*, 122375. [CrossRef]
95. Zhang, D.; Qu, X.; Yang, X.; Zhao, Y.; Meng, H. Rebar clutter suppression method based on range migration compensation and low-rank and sparse decomposition. *IEEE Trans. Geosci. Remote Sens.* **2023**, *61*, 5110213. [CrossRef]
96. Dehmollaian, M.; Thiel, M.; Sarabandi, K. Through-the-wall imaging using differential SAR. *IEEE Trans. Geosci. Remote Sens.* **2009**, *47*, 1289–1296. [CrossRef]
97. Tivive, F.H.C.; Bouzerdoum, A.; Amin, M.G. A subspace projection approach for wall clutter mitigation in through-the-wall radar imaging. *IEEE Trans. Geosci. Remote Sens.* **2015**, *53*, 2108–2122. [CrossRef]
98. Eltrass, A.S. An enhanced approach for clutter removal and target imaging in throughwall radar systems. In *Proceedings of the 2018 IEEE Conference on Antenna Measurements & Applications (CAMA)*; IEEE: New York, NY, USA, 2018; pp. 9–12. [CrossRef]
99. Candès, E.J.; Li, X.; Ma, Y.; Wright, J. Robust Principal Component Analysis? *J. ACM* **2011**, *58*, 11. [CrossRef]
100. Chen, M.; Hu, X.; Wu, Y. Clutter suppression in through-the-wall radar based on low-rank and sparse. In *Proceedings of the 2025 8th International Conference on Information Communication and Signal Processing (ICICSP)*; IEEE: New York, NY, USA, 2025; pp. 72–76. [CrossRef]
101. Tivive, F.H.C.; Bouzerdoum, A. Clutter removal in through-the-wall radar imaging using sparse autoencoder with low-rank projection. *IEEE Trans. Geosci. Remote Sens.* **2021**, *59*, 1118–1129. [CrossRef]
102. Bivalkar, M.; Singh, D.; Kobayashi, H. Entropy-based low-rank approximation for contrast dielectric target detection with through wall imaging system. *Electronics* **2019**, *8*, 634. [CrossRef]
103. Wang, G.; Amin, M.G. Imaging through unknown walls using different standoff distances. *IEEE Trans. Signal Process.* **2006**, *54*, 4015–4025. [CrossRef]

104. Ahmad, F.; Amin, M.G.; Mandapati, G. Autofocusing of through-the-wall radar imagery under unknown wall characteristics. *IEEE Trans. Image Process.* **2007**, *16*, 1785–1795. [CrossRef] [PubMed]
105. Jin, T.; Chen, B.; Zhou, Z. Image-domain estimation of wall parameters for autofocusing of through-the-wall SAR imagery. *IEEE Trans. Geosci. Remote Sens.* **2013**, *51*, 1836–1843. [CrossRef]
106. Singh, A.P.; Singh, V. A novel hybrid autofocusing technique for compressive sensing-based through-the-wall radar imaging with synthetic aperture radar system. *IEEE Sens. Lett.* **2025**, *9*, 3506604. [CrossRef]
107. Ma, Y.; Hong, H.; Zhu, X. Interaction multipath in through-the-wall radar imaging based on compressive sensing. *Sensors* **2018**, *18*, 549. [CrossRef] [PubMed]
108. Zhu, Z.; Chen, J.; Guo, S.; Cui, G.; Yang, X. Compressive sensing-based two-step multipath suppression method for MIMO through-the-wall radar imaging. In *Proceedings of the 2024 IEEE International Geoscience and Remote Sensing Symposium (IGARSS), Athens, Greece, 7–12 July 2024*; IEEE: New York, NY, USA, 2024; pp. 8912–8915. [CrossRef]
109. Liao, J.; Zeng, X.; Yang, X.; Yin, Z.; Zhao, J. Indoor target multipath ghost suppression method based on virtual array rotation. *IEEE Trans. Aerosp. Electron. Syst.* **2026**, *62*, 7958–7973. [CrossRef]
110. Le, C.; Dogaru, T.; Nguyen, L.; Ressler, M.A. Ultrawideband (UWB) radar imaging of building interior: Measurements and predictions. *IEEE Trans. Geosci. Remote Sens.* **2009**, *47*, 1409–1420. [CrossRef]
111. Li, W.; Tang, H.; Huan, C.; Zhang, F.; Chen, L. A novel standing wave ghost-suppression approach for UWB through-the-wall SAR imaging. *Electronics* **2026**, *15*, 1713. [CrossRef]

Disclaimer/Publisher's Note: The statements, opinions and data contained in all publications are solely those of the individual author(s) and contributor(s) and not of MDPI and/or the editor(s). MDPI and/or the editor(s) disclaim responsibility for any injury to people or property resulting from any ideas, methods, instructions or products referred to in the content.